X-ray Photoelectron Spectroscopy (XPS) Study of Layered Double Hydroxides with Different Exchangeable Anions

J. Theo Kloprogge *

Posted Date: 10 January 2025

doi: 10.20944/preprints202501.0802.v1

Keywords: X-ray Photoelectron Spectroscopy; layered double hydroxide; LDH; interlayer anion

Article

X-ray Photoelectron Spectroscopy (XPS) Study of Layered Double Hydroxides with Different Exchangeable Anions

J. Theo Kloprogge

Department of Chemistry, College of Arts and Sciences, University of the Philippines Visayas, Miagao, Iloilo 5023, Philippines; theoklop@bigpond.com

Abstract: Layered double hydroxides (LDH) containing various exchangeable anions were studied to show how X-ray Photoelectron Spectroscopy (XPS) can provide information on the local environments of the different elements within the interlayer anionic groups and their possible influence on the LDH interlayer hydroxide surfaces. As such XPS can potentially provide additional information about these systems that cannot be obtained by other common spectroscopic methods such as infrared and Raman spectroscopy. A $Mg_6Al_2X(OH)_{16}.4H_2O$ with X representing interlayer anions CO_3^{2-}, PO_4^{3-}, SO_4^{2-}, MoO_4^{2-}, CrO_4^{3-}, $Fe(CN)_6^{4-}$, and $Fe(CN)_6^{3-}$ was studied. The hydroxide layer structure is characterized by the Mg 2p and Al 2p with a binding energy of around 50.1 and 74.5 eV for the normal CO_3^{2-} containing LDH. The O 1s contained three peaks related to the layer OH-groups at 531.6 eV, interlayer CO_3^{2-} at 530.5 eV and interlayer water at 532.4 eV. Similar observations were made for the other interlayer anions showing characteristic P 2p, S 2p, and Mo 3d peaks. Intercalation with CrO_4^{3-} shows that a significant amount of the Cr^{6+} has been reduced to Cr^{3+}. Finally, the intercalation of hexacyanoferrate in hydrotalcite showed the potential of XPS in detecting changes in the oxidation state of Fe upon intercalation in the LDH with a change in the Fe 2p peaks with a shift in binding energy and the possibility to determine the amount of reduction of Fe(III) to Fe(II). In general, the XPS high resolution scans of P 2p, S 2p, Mo 3d, and Cr 2p show that slightly lower binding energies are observed compared to the binding energy values for the corresponding anionic groups as part of a rigid crystal structure, such as in minerals. Overall, the influence of the nature of the interlayer anion on the binding energy of the elements (Mg, Al, O) in the layered double hydroxide structure is minimal and considered to be within the experimental error of XPS. Detailed analysis of XPS data in combination with infrared and Raman spectroscopy show how XPS can provide additional information not readily available via vibrational spectroscopy.

Keywords: X-ray photoelectron spectroscopy; layered double hydroxide; LDH; interlayer anion

1. Introduction

Hydrotalcites, also referred to as layered double hydroxides (LDHs), are categorized as anionic clays due to their distinctive layered architecture [1,2]. This structure is characterized by positively charged hydroxy layers, in stark contrast to cationic (silicate) clays such as smectites, which possess a negative layer charge. Within the interlayer space of these positively charged layers, anions are present to balance the overall charge. A more comprehensive understanding of hydrotalcite's structure reveals positively charged hydroxide layers that resemble those found in brucite [$Mg(OH)_2$]. In this configuration, a portion of the Mg^{2+} ions can be substituted with trivalent metals, such as Al^{3+}, while charge-compensating anions, typically in a hydrated form, occupy the interstitial regions between the hydroxide layers [2,3].

The composition of LDH is very versatile, commonly represented by the formula $[M^{2+}_{1-x}M^{3+}_x(OH)_2][A^{n-}]_{x/n}\cdot yH_2O$, where M^{2+} and M^{3+} denote the divalent and trivalent cations residing in octahedral coordination within the hydroxide layers. The variable x usually ranges from 0.17 to 0.33,

 doi:10.20944/preprints202501.0802.v1

indicating the proportion of M^{3+} ions. Notably, it is imperative that the ionic radii of M^{2+} and M^{3+} do not exhibit significant disparity—specifically, a deviation of no more than 30%—to maintain structural integrity. For instance, the ionic radii for Mg^{2+} and Al^{3+} are approximately 0.65 Å and 0.45 Å, respectively. Furthermore, sound chemical principles dictate that the solubility products, S_1 for $M^{2+}(OH)_2$ and S_2 for $M^{2+}CO_3$, must adhere to the conditions where the difference $pS_1 - pS_2$ is maintained within the range of 0 and 10, ensuring the stability of the hydrotalcite phase [2–4].

The variety of anions that can exist within the LDH framework is relatively unconstrained, provided that these anions do not engage in complexation with the cations within the octahedral sheets during the synthesis process. Such complexation would inhibit the formation of a viable LDH structure [5]. The inherent flexibility in both cationic and anionic compositions of hydrotalcites enables the engineering of tailor-made materials suitable for a broad array of applications. These may include their utilization as basic catalysts or precursors for synthesizing mixed metal oxide catalysts. Additionally, hydrotalcites serve functional roles as adsorbents, fillers, UV stabilization agents, chloride scavengers, and thermal stabilizers, positioning them as versatile components in various industrial and technological contexts [6–11].

Infrared spectroscopy, along with the less frequently employed Raman spectroscopy, has proven instrumental in elucidating the structural and compositional characteristics of LDH containing varied cations and anions. These spectroscopic techniques have facilitated comprehensive examinations of anionic intercalation and thermal degradation processes in these materials, primarily serving to identify a range of exchangeable anions. Among the anions detected in such studies are carbonate (CO_3^{2-}), chloride (Cl^-), perchlorate (ClO_4^-), nitrate (NO_3^-), sulfate (SO_4^{2-}), arsenate (AsO_4^{3-}), vanadate (VO_4^{3-}), molybdate (MoO_4^{2-}) and chromate (CrO_4^{2-}) [12–27]. Moreover, the investigation has extended to more complex anionic entities, including anionic silica ($SiO(OH)_3^-$) [28] and larger polyoxometalate ions as well as hexacyanoferrate complexes ($Fe(CN)_6^{n-}$) [see e.g., [29,30–35]].

The unique vibrational fingerprints associated with each of these anions are discernible through their respective infrared and Raman spectra. These spectral signatures provide crucial insights into the interactions and substitutions occurring within the hydrotalcite matrix. Through rigorous analysis using these spectroscopic techniques, researchers have been able to correlate the presence of specific anions with structural modifications within the LDH framework. This knowledge not only enhances the understanding of the properties of LDH but also informs potential applications in fields such as catalysis, ion exchange, and environmental remediation, where the selective uptake and release of ions play a critical role. Such advancements underscore the relevance of infrared and Raman spectroscopy in characterizing the multifaceted nature of hydrotalcites and their layered structures.

X-ray photoelectron spectroscopy (XPS) has established itself as the predominant technique for investigating surface phenomena. However, there remains a notable paucity of research focusing on the bulk atomic structure and chemical states of minerals. This oversight is particularly striking given that the vast majority—often exceeding 90%—of the intensity of XPS lines is derived from the bulk material when employing conventional laboratory X-ray sources, such as the Al Kα source at 1486.6 eV. This discrepancy invites further inquiry into the collective properties of minerals that are not fully captured by surface-centric methodologies.

Historically, the XPS analysis of various mineralogical components has been documented in the literature, encompassing a diverse range of materials including feldspars, clays, aluminum oxy(hydroxide) phases, arsenates, and phosphates. Notable contributions have highlighted the unique electronic and structural characteristics present in these minerals, but comprehensive studies that simultaneously account for both surface and bulk properties remain limited. It is essential to broaden the scope of investigation to include these often-ignored bulk properties to achieve a better understanding of mineral behavior. So far, limited use has been made of XPS as an analytical tool to study LDH in detail and generally stops at just providing binding energy values [see e.g., [36,37–42]]. As part of an ongoing study on LDH this study aims to better understand the X-ray photoelectron

 doi:10.20944/preprints202501.0802.v1

spectroscopy (XPS) of the interlayer anions in LDH to complement the existing Infrared and Raman spectral data of LDH.

2. Materials and Methods

The synthesis of hydrotalcite, characterized by the theoretical composition $Mg_6Al_2(OH)_{16}CO_3.nH_2O$, was performed utilizing the procedure outlined by Kloprogge and Frost [43]. The procedure involves the gradual simultaneous introduction of a solution containing aluminum nitrate (0.25 M) and magnesium nitrate (0.75 M) alongside a mixed solution of NaOH (2.00 M) and Na2CO3 (0.125 M), while vigorous stirring. The pH is maintained at approximately 10 throughout the process. The product was washed to eliminate excess salt and dried at 60 °C.

To minimize the incorporation of carbonate during the synthesis of hydrotalcites with other anions, several measures were employed: deionized water was boiled prior to use, NaOH pellets were thoroughly rinsed, and the synthesis was conducted in a nitrogen atmosphere. A mixed solution containing aluminum and magnesium nitrates was prepared with concentrations of $[Al^{3+}]$ at 0.25 M and $[Mg^{2+}]$ at 0.75 M. Additionally, a separate mixed solution of sodium hydroxide was formulated with a hydroxide concentration of $[OH^-]$ at 2 M, incorporating the desired anion at the specified concentration. Both solutions were transferred into distinct vessels and subjected to nitrogen purging for 20 minutes, with all solutes dissolved in freshly decarbonated water. The cationic solution was delivered to the anionic phase using a peristaltic pump at a flow rate of 40 mL/min, while maintaining the pH above 9. The resulting mixture was subjected to aging at 75 °C for 18 hours in a nitrogen atmosphere. Following this, the precipitate was filtered using room temperature decarbonated water to eliminate nitrate ions and subsequently dried in a vacuum desiccator over several days. This method facilitated the synthesis of hydrotalcites containing various anions in the interlayer. Phase composition was evaluated via X-ray diffraction, and chemical composition was determined through energy-dispersive X-ray spectroscopy (EDXA) analyses [44].

X-ray photoelectron spectroscopy (XPS) data were acquired on a Kratos AXIS Ultra (Kratos Analytical, Manchester, U.K.) utilizing a monochromatic 225 W Al X-ray source and conducted under ultrahigh vacuum conditions. Initial survey scans were executed within the energy range of 0 to 1200 eV, employing a dwell time of 100 milliseconds, a pass energy of 160 eV, and a step size of 1 eV over a single sweep. Subsequent high-resolution analyses were performed by increasing the number of sweeps, reducing the pass energy to 20 eV with a step increment of 100 meV, and extending the dwell time to 250 milliseconds. For calibration purposes, the adventitious C 1s peak at 284.8 eV was utilized to correct all spectra.

3. Results

3.1. Layer Structure

Figure 1 shows the survey scan for a normal LDH with carbonate as the interlayer anion. It is characterized by a single Mg 2p peak at 50.1 eV, a single Al 2p peak at 74.5 eV (Figure 2), as well as a single O 1s peak at 531.6 eV. High resolution scans of the O 1s exhibits three peaks at 530.5 eV, 531.6 eV and 532.4 eV assigned to oxygen atoms in the interlayer carbonate anion-, hydroxyl groups and interlayer water, respectively. These values are in excellent agreement with the results reported by Kloprogge and Wood [45]. They also showed the Mg 2p for $Mg(OH)_2$ at 49.3 eV, which is at a slightly lower binding energy (BE) than for LDH as shown here, caused by the partial substitution of Mg^{2+} by Al^{3+}. The LDH Al 2p peak at 74.5 eV is close to the BE observed for gibbsite, $Al(OH)_3$ (74.4 eV), bayerite, $Al(OH)_3$ (75.0 eV), boehmite (73.9 eV), AlOOH, and pseudoboehmite, AlOOH (74.3 eV) [46]. Peng, *et al.* [47] observed comparable BE values for LDH with Mg 2p at 50.29 eV, Al 2p at 74.31 eV.

 doi:10.20944/preprints202501.0802.v1

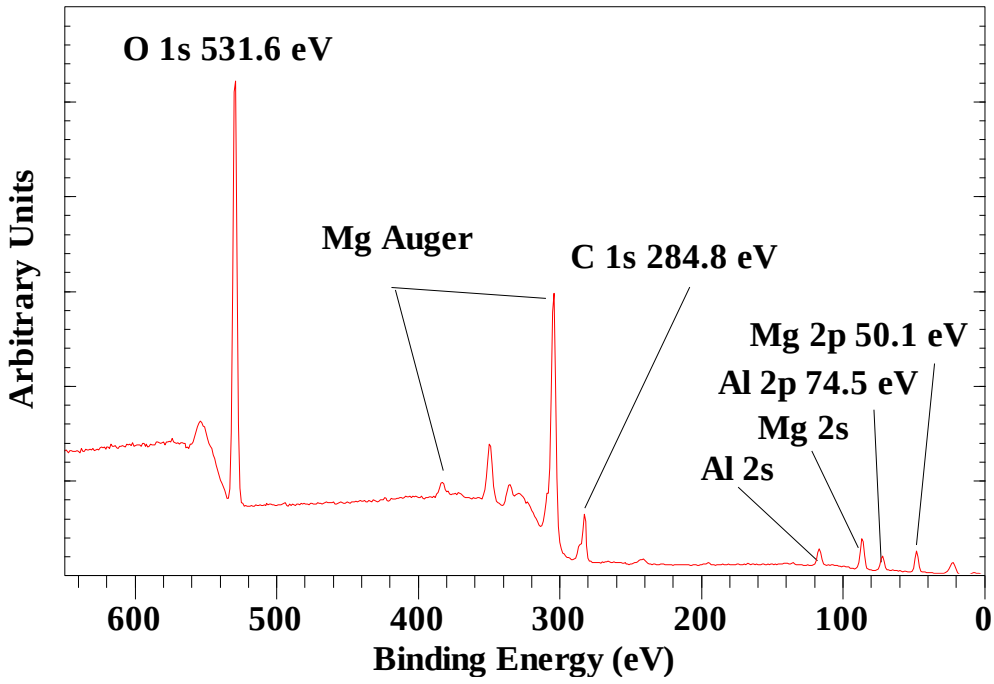

Figure 1. XPS survey scan of LDH with carbonate as the anion in the BE region between 650-0 eV. The region between 1200 and 650 is not shown as no peaks are observed there.

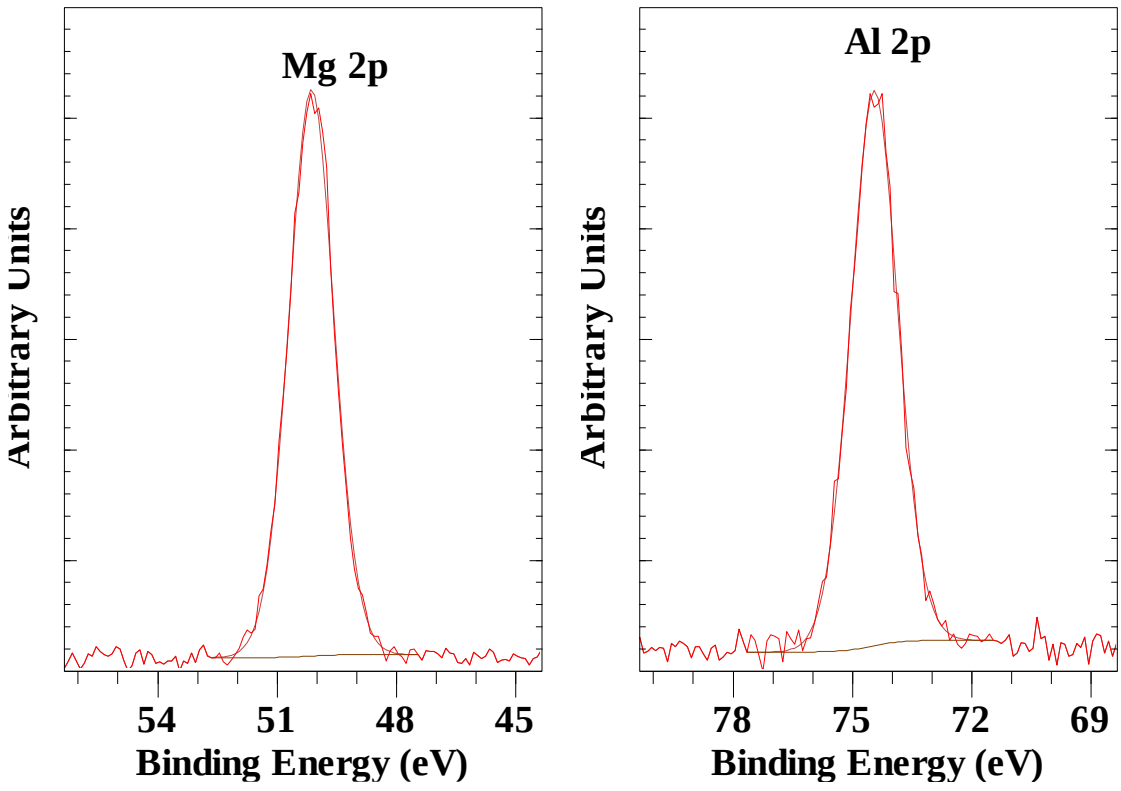

Figure 2. XPS high resolution scan of Mg 2p and Al 2p of LDH with carbonate as the anion.

 doi:10.20944/preprints202501.0802.v1

3.2. Carbonate Anion

The most often studied interlayer anionic group in LDH, due to its strong affinity to the hydroxide layers, is CO_3^{2-}. Going from the free anion in solution changes can be anticipated when the CO_3^{2-} is present in the interlayer space of LDH due to interactions with interlayer H_2O and/or OH groups at the interlayer surfaces of the LDH layers.

The C 1s high resolution spectrum of the carbonate anion shows a peak at a BE value of 288.6 eV (Figure 3 left). This peak is due to the interlayer anion. The other peaks are due to surface adsorbed organic matter, the socalled "rubbish" carbon.The corresponding O 1 peak was found at 530.5 eV (Figure 3 right) and the ratio of O/C is about 3.10, close to the expected ratio of 3 for CO_3^{2-}. The BE value is slighlty lower compared to pure carbonate minerals such as magnesite which has a C 1s at 290.0 eV, dolomite 289.8 eV, and calcite 289.5 eV [45]. This shift in BE is probaly associated with interactions with the interlayer water molecules and the restrictions imposed by the LDH layers.

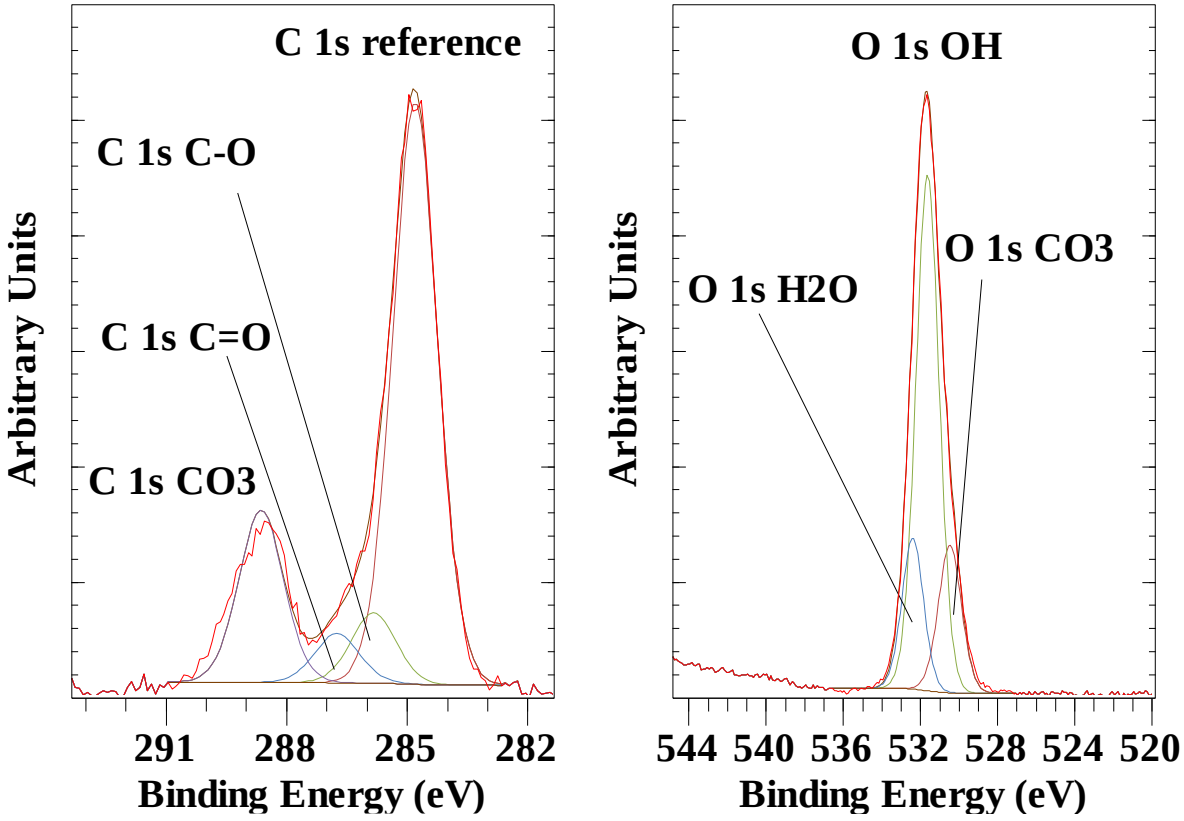

Figure 3. XPS high resolution scan of C 1s and O 1s of LDH with carbonate as the interlayer anion.

In earlier work Kloprogge, Wharton, Hickley and Frost [19] have shown by infrared and Raman spectroscopy that there is an interaction with interlayer water as shown by a water-carbonate bridging mode around 3000-3100 cm^{-1}. Rey, *et al.* [48] observed that heating Mg/Al-LDH to 100 °C resulted in the disappearance of this water-carbonate bridging mode together with the water OH-bending mode around 1616 cm^{-1} due to dehydration. Relative to free CO_3^{2-} a shift toward lower wavenumbers was detected. Based on X-ray diffraction, ionic size, and charge density, it has been generally accepted that the CO_3^{2-} anion is present within the interlayer space with its C_3 axis perpendicular to the interlayer surfaces of the LDH hydroxide layers [49].Due to these restrictions in the interlayer space the symmetry of the carbonate anion decreased from D_{3h} to C_{2s} causing the activation of the IR inactive ν_1 mode around 1050–1060 cm^{-1}. In addition, the ν_3 showed a splitting of 30–60 cm^{-1}.Though IR and Raman clearly show that there are interactions between the interlayer

 doi:10.20944/preprints202501.0802.v1

anion and the LDH layers as well as water and that the movement of the interlayer anion is restricted, XPS shows that the binding energy of the C 1s is less than for a pure carbonate mineral indicative that the carbonate anion still has some degree of freedom inside the interlayer space.

3.3. Phosphate Anion

The interlayer phosphate anion is characterized by the P 2p3/1 peak with a BE of 133.0 eV. The corresponding P 2p1/2 is found at a BE value of 132.1 eV (Figure 4 left). The synthesis of the phosphate containing LDH was performed at 3 different pH values (9.3, 11.9 and 12.5). No difference in the BE values was observed but a significant higher amount of phosphate was present in the interlayer space of the LDH in th lowest pH sample. The BE value is similar to some common phosphate minerals, such as monazite, autunite, vivianite and apatite, which have P 2p3/2 Be values around 133.2 to 134 eV [50]. On the other hand the BE of H_3PO_4 is slightly higher than observed here at 135.2 eV. The same is true for NaH_2PO_4 with a BE of 134.0 to 134.2 eV [51]. Wang, Cai, Han, Fang, Chen and Tan [22] reported the P 2p at approximately 134 eV for LDH containing hexametaphosphate. At the same time they observed a shift in the Mg 2p and Al 2p towards higher BE. They ascribed this shift in BE to the fact that the Mg^{2+}/Al^{3+} in the LDH hydroxide layers can extract electron density from the negatively charged oxygen atoms in hexametaphosphate [52]. Gupta, Saifuddin, Kim and Kim [52] found a BE shift in the Zn 2p of 0.04 eV which is considered to be within the experimental error of XPS, while the Fe 2p showed a larger shift in BE of about 0.2 eV. In this study no shift was observed for the Mg 2p, and a minor shift toward a higher BE value of 0.1 eV for the Al 2p.

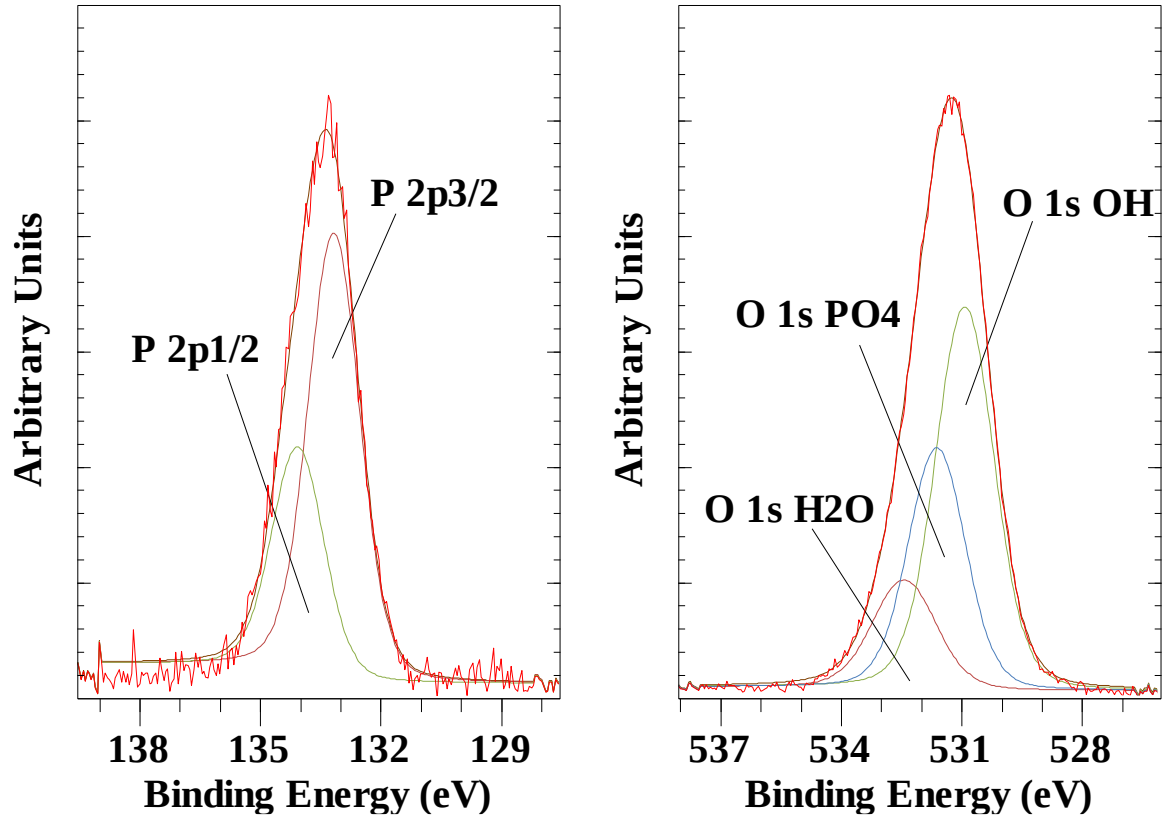

Figure 4. XPS high resolution scan of P 2p and O 1s of LDH with phosphate as the interlayer anion.

The O 1s is characterized by three peaks associated with the layer hydroxyl groups at 530.9 eV, interlayer water at 532.4 eV and the interlayer PO_4^{2-} at 531.6 eV (Figure 4 right). Again the BE value for the oxygen in the phosphate anion is comparable to that found for various phosphate minerals, e.g., monazite (531.2 eV), vivianite (531.2 eV), amblygonite (531.6 ev) and apatite (531.0 eV) [50]. Similar BE values are also listed in the NIST database, with e.g., $AlPO_4$ at 532.8 eV [51]. Wang, Cai,

 doi:10.20944/preprints202501.0802.v1

Han, Fang, Chen and Tan [22] only reported a general position for the O 1s at about 532 eV, but did not attempt to provide details fitting of the different oxygen species present. Gupta, Saifuddin, Kim and Kim [52] fitted the O 1s with three bands with the O 1s OH at 530.1 eV, slightly lower than observed here. In contrast though, the other two peaks are at very different BE values with an extremely broad peak at 530.9 eV assigned to H_2O, -O-Nand O-C, while a third peak at very low BE of 528.4 eV assigned to M-O. No explanation is given for what M is but presumebaly this is the P-O in the phosphate as there are no M-O modes in the LDH hydroxyde layer. These assignments don't seem to be correct as generally O 1s for PO_4 is always found at much higher BE.

LDHs intercalated with PO_4^{3-} have been shown to form different phases with very different basal spacings: 0.84 nm [20], and 0.78 nm, 0.80 nm, 1.19 nm [17] and 1.11 nm [53], depending on the synthesis conditions such as Mg/Al ratio, pH, etc.. This spread in basal spacings can be explained by different positions adopted by the PO_4^{3-} between the LDH hydroxyde layers (perpendicular, inclined and planar). Wang, Cai, Han, Fang, Chen and Tan [22] even indicate that the hexametaphosphate complex stays intact within the interlayer space of the LDH after exchange. Mid-infrared and Raman spectra have been reported in a limited number of papers. Benício, *et al.* [54] reported the IR-active bands in the 1050 cm^{-1}, 870 cm^{-1} and 550 cm^{-1} regions, which correspond to ν_3, ν_1, and ν_4 vibrations [55,56]. The PO_4^{3-} anion is tetrahedral with T_d symmetry, thus there are four normal modes of vibration, all of which are Raman active. However only the triply degenerate $\nu_3(F_2)$ and $\nu_4(F_2)$ modes are infrared active. The observation of the ν_1 mode must be due to either the presence of some nitrate or carbonate instead [19]. In contrast, Benício, Constantino, Pinto, Vergütz, Tronto and Da Costa [53] in a paper a year earlier claim the presence of not only PO_4^{3-} in the interlayer space but also HPO_4^{2-}. Though the spectrum provided is of rather low quality and they don't show the band fit, they claim that the broad band in the 1020 cm^{-1} region, consists of the ν_3 vibrational mode of PO_4^{3-} anion and two additional bands assigned to the ν_3 and ν_2 modes of HPO_4^{2-} anion [57]. In contrast, Gupta, Saifuddin, Kim and Kim [52] assigned the bands at 1045 cm^{-1} and 565 cm^{-1} corresponding to the ν_3 and ν_4 band vibrations of HPO_4^{2-} or $H_2PO_4^-$ without further explanation. Wang, Cai, Han, Fang, Chen and Tan [22] reported only a single band at 1088 cm^{-1} attributed to the vibration of P-O. Shabanian, *et al.* [58] reported that three bands attributedto HPO_4^{2-} coalesce into a single broad band around 1056 cm^{-1}. In addition, a shoulder band was detected at 870 cm^{-1} near the theoretical antisymmetric stretching mode of P–OH. Others also described the characteristic band related to phosphate in the interlayer of Zn/Al LDH at 1040 cm^{-1} [59] and 1048 cm^{-1} [60].

In earlier work we reported on the Raman spectra of phosphate-LDH and addressed the possibility of determining the presence of $H_2PO_4^-$ and HPO_4^{2-} in addition to PO_4^{3-} [17]. The Raman spectra will change if hydrogen is linked to the phosphate unit as the symmetry will change from T_d to C_{3v} to C_{2v}. This will cause a loss of degeneracy and other bands may become visible. The sample synthesised at pH 12.5 exhibited an strong sharp band at 960 cm^{-1} with a broader band at 1026 cm^{-1} assigned to the PO_4^{3-} symmetric and antisymmetric stretching vibrational modes identical to that of the PO_4^{3-} ion. Similar bands were observed for the pH 11.9 sample at 957 cm^{-1} and 1032 cm^{-1}. Benício, Eulálio, Guimarães, Pinto, Costa and Tronto [54] reported the formation of bands in the region between 940 cm-1 and 960 cm-1 after exchange with phosphate. Slight changes were also deted in the band positions in the 1050 cm^{-1} region. A different Raman spectrum was obtained for the pH 9.3 sample with four bands at 964, 989, 1033 and 1138 cm^{-1}. In aqueous systems the PO_4^{3-} ion has a strong band at 936 cm^{-1}, while HPO_4^{2-} anion exhibits a strong band at 990 cm^{-1}. Therefore the spectrum can be interpreted as being a combination of the PO_4^{3-} anion (964 and 1033 cm^{-1}) and the HPO_4^{2-} ion (989 and 1138 cm^{-1}). However it is questionable whether these are actually present in the interlayer space of LDH as XRD showed the material mainly as amorphous. For the oxyanion PO_4^{3-} the symmetric bending mode (ν_2) and the ν_4 mode are observed at 420 cm^{-1} and 567 cm^{-1}, respectively. For the phosphate LDH at pH 12.5 a band at 474 cm^{-1} was observed. A similar band was found at, 472 cm^{-1} for the pH 11.9 sample, while a broad band around 441 cm^{-1} was present in the Raman spectrum of the pH 9.3 sample.

 doi:10.20944/preprints202501.0802.v1

Infrared and Raman spectroscopy of phosphate-LDH has shown that the nature of the anion present in the interlayer space is affected by the synthesis conditions. In this study three different pH values were studied. Despite the fact that in the literature the presence of $H_2PO_4^-$ and HPO_4^{2-} have been claimed [52,53]. For the two samples synthesised at pH 12.5 and 11.9 this was shown not to be the case by Raman spectroscopy [17]. This is further confirmed by the XPS results that show only a single P 2p 3/2 peak as well as by the O/P ratio which in both cases is close to 4. XPS did not allow to distinguish between PO_4^{3-} and HPO_4^{2-} in the three samples studied.

3.4. Sulphate Anion

In naturally occurring LDH, other than the commonly present CO_3^{2-} anion, SO_4^{2-} forms an additional important interlayer anion found in minerals such as honessite ($Ni_6Fe_2SO_4(OH)_{16}\cdot 4H_2O$), hydrohonessite ($Ni_6Fe_2SO_4(OH)_{16}\cdot 7H_2O$), and carrboydite ($(Ni,Cu)_{14}Al_9(SO_4,CO_3)_6(OH)_{43}\cdot 7H_2O$) [61–63]. Figure 5 shows the S 2p and O 1s of sulphate-LDH. The S 2p is characterized by a single S 2p3/1 peak with a BE of 168.3 eV. This BE is slighly lower than observed for common sulphate minerals such as baryte (169.2 eV), anhydrite (168.9 eV), or gypsum (169.2 eV) [45], indicating that the sulphate in the LDH interlayer space is less strongly interacting with the LDH hydroxide layers compared to a sulphate group in a rigid crystal structure. In the O 1s a single peak at 532.4 eV is associated not only with the oxygen in the sulphate group but also with oxygen in interlayer water that has a similar BE. This value is comparable with H_2SO_4 which has an O 1s BE of 532.5 eV and $Al_2(SO_4)_3$ of 532.4 eV [51]. Similar results were also reported for group 1A sulphates by Wahlqvist and Shchukarev [64]

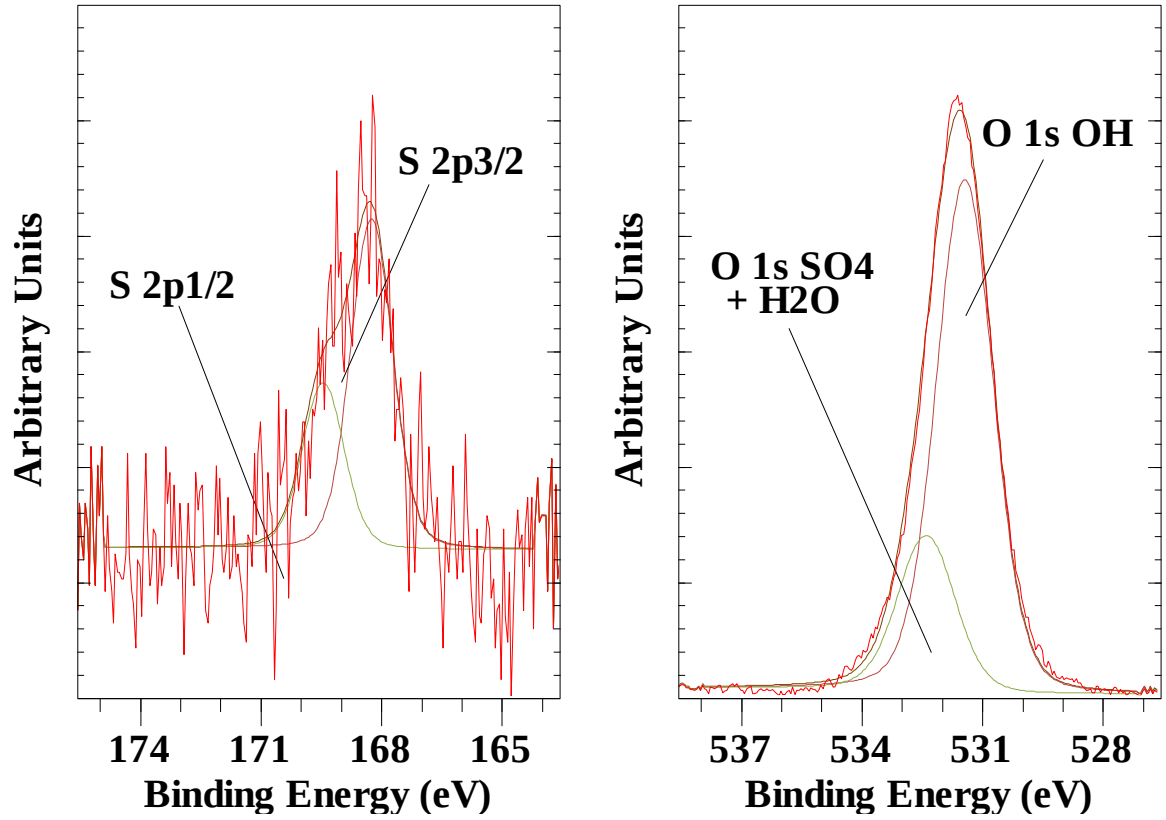

Figure 5. XPS high resolution scan of S 2p and O 1s of LDH with phosphate as the interlayer ani-on.

Bish and Livingstone [61] described for honessite the SO_4^{2-} ν_1, ν_2, ν_3, and ν_4 infrared active modes at 980, 500, 1140, and 650 cm^{-1}, respectively. The ν_3 mode is obviously split though no separate band positions were provided. Since all four modes are infrared active the symmetry of the SO_4^{2-} anion was lowered from T_d (free anion) to either C_3 or C_{3v}, causing the activation of the two infrared inactive modes together with the splitting of the ν_3 mode [65]. Earlier work in our group has shown that the

 doi:10.20944/preprints202501.0802.v1

infrared spectrum of Mg/Al-LDH containing SO_4^{2-} in the the interlayer space exhibits a strong but broad ν_3 mode at 1126 cm^{-1}, a ν_4 mode at 614 cm^{-1}, and a very weak ν_1 mode at 981 cm^{-1} [19]. The ν_2 mode was not observed as a distinct band, in contrast to honessite and hydrohonnesite, due to its overlap with the O-M-O bending vibration of the LDH hydroxide layer around 450 cm^{-1} [66]. Fahami and Beall [67] reported only a band at a significantly lower wavenumber position around 1066 cm^{-1} were attributed to the bending mode of interlayer sulfate ions. Liu and Yang [68] described a single band for Zn/Al-LDH at 1113 cm-1 which is much closer to the value observed by Kloprogge, Wharton, Hickley and Frost [19]. Frost, *et al.* [69] described for glaucocerinite $(Zn,Cu)_{10}Al_6(SO_4)_3(OH)_{32}\cdot 18H_2O$, a naturally occurring LDH mineral, three strong bands at 1053, 1078 and 1109 cm^{-1} which was attributed to the SO_4^{2-} ν_3 antisymmetric stretching mode. A weak band at 986 cm^{-1} was assigned to the correcsponding ν_1 symmetric stretching mode. They also reported that carrboydite exhibted three similar bands at 1088, 1021 and 978 cm^{-1} with the first two bands due to ν_3 antisymmetric stretching modes and the last band to the ν_1 symmetric stretching mode.

Kloprogge, Wharton, Hickley and Frost [19] showed that the Raman spectrum of sulphate-LDH consisted of a very intense ν_1 mode at 982 cm^{-1} together with medium intensity ν_2 and ν_4 modes around 453 and 611 cm^{-1}, respectively. The ν_3 mode was not observed as a separate band, even though a broad bandwas visible around 1134 cm^{-1}. They indicaed that when SO_4^{2-} is located in the interlayer space of LDH the infrared ν_2 mode may become inactive, while at the same time the ν_1 mode becomes active. In contrast to the other modes the ν_3 is considerably broader indicating the possible existence of two overlapping bands due to splitting. Dutta and Puri [70] proposed a D_2 site symmetry for the sulphate anion. This is not compatible with the infrared spectrum where all four modes are present. For analogous reasons the C_3 site symmetry as propsed by Bish [71] is not compatible with the Raman spectrum. Hence, using the combined observations in both the infrared and Raman spectra Kloprogge, Wharton, Hickley and Frost [19] conclued that the site symmetry is most probably C_{2v} with ν_1 infrared and Raman active, ν_2 infrared and Raman active, and ν_3 and ν_4 infrared and Raman active. A similar conclusion was reached by Lin, *et al.* [72] for $Ni_xZn_{6-x}Al_2(OH)_{16}(SO_4)\cdot 4H_2O$, while Frost, Theiss, López and Scholz [69] concluded for glaucocerinite a reduction in symmetry of the sulphate anion from T_d to C_{2v} or even lower symmetry.

It is clear from the infrared and Raman data that the sulphate anion when present in the interlayer space is restricted in its movement and has a lower site symmetry due to the interactions with the LDH hydroxide layers. This is also reflected in the XPS data where the S 2p clearly shows a slightly lower BE compared to structural sulphate in mineral structures. This confirms that the sulphate anion is no longer a completely free anion, but it is to a certain extent interacting with the hydroxide layers.

3.5. Molybdate Anion

The MoO4-LDH is characterized by a single peak for the Mo 3d5/2 at a BE of 229.6 eV (Figure 6 left). This BE value is lower than e.g molybdenite, MoS_2, with a BE of 230.1 eV or wulfenite, $PbMoO_4$, with a BE of 231.9 eV [3]. Several molybdates, such as $Al_2(MoO_4)_3$ (232.5 eV), $CaMoO_4$ (232.8 eV), $NiMoO_4$ (233.0), etc. all have higher BE than observed for intercalated molybdate ions in LDH. This is similar to what has been observed before, an indication that the interactions between the molybdate anion and th LDH hydroxide layers are not as strong as when the molybdate is part of a rigid crystal structure. The corresponding O 1s peak is observed at 530.3 eV (Figure 6 right), which compares well with the value observed for wulfenite at 530.0 eV. The NIST database reports for H_2MoO_4 a BE of 530.7 eV, $CaMoO_4$ at 530,6 eV, $NiMoO_4$ at 530.9 eV, while for $Al_2(MoO_4)$ the BE ranges from 530.7 to 531.0 eV [51]. Thao, *et al.* [73] assigned the Mo 3d5/2 peak at 232.6 eV to Mo(VI) in MoO_4^{2-}. The hardly visible shoulder at 231.7 eV was attributed to Mo(V) species possibly caused by a charge transfer between (Mo^{6+} + O^{2-}) and (Mo^{5+} + O^{-}) [74,75]. This shoulder was not observed in this study. Thao, Trung and Van Long [73] also reported the BE value of O 1s at 532.4 eV for the fresh molybdate-LDH assigned to the O^{2-} [35,38,45]. They concluded that it is probably composed of two overlapping photoelectron peaks at 532.4 and 531.5 eV. The peak at 532.4 eV was assigned to the metal hydroxides

 doi:10.20944/preprints202501.0802.v1

in the LDH layers, while the other peak at 531.6 eV was attributed to oxygen O^- in the oxomolybdenum. Both the Mo 3d5/2 and O 1s peaks for the MO42- anion are at slighly higher BE values than observed in this study and in comparison with other molybdate structures such as listed in Kloprogge and Wood [45] and the NIST database [51].

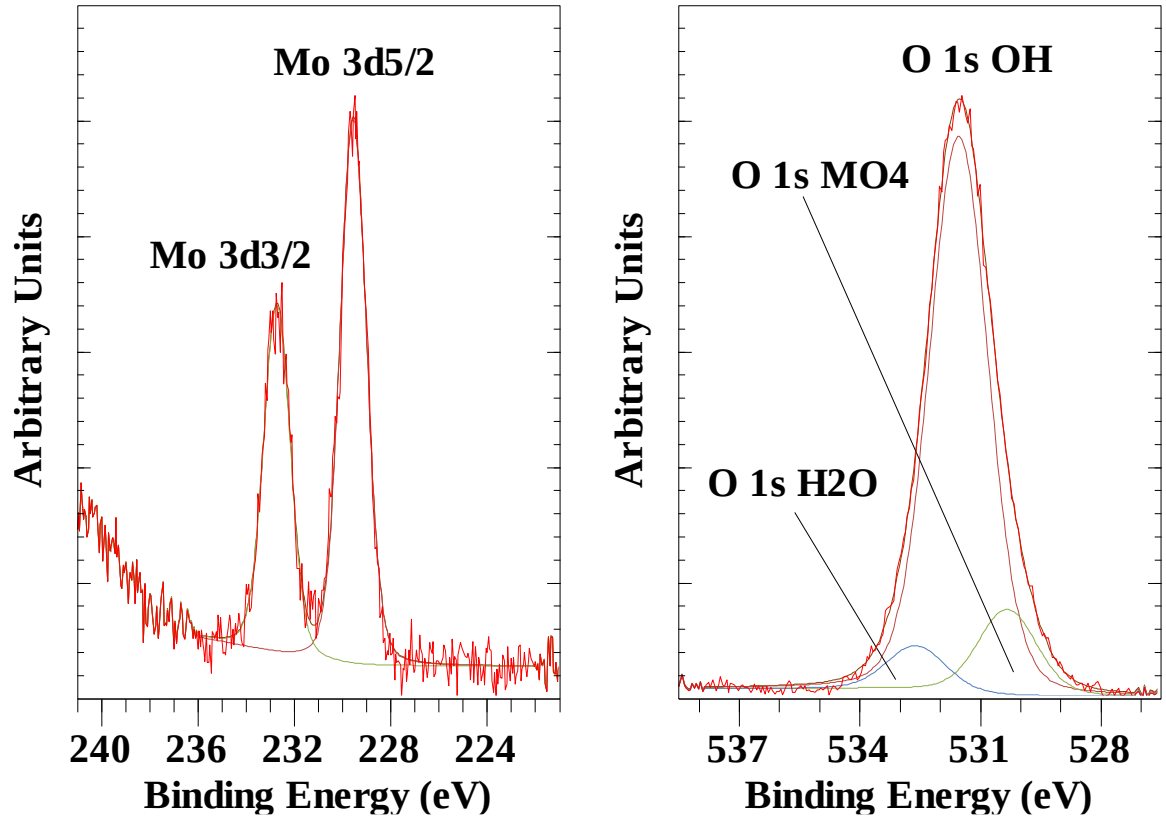

Figure 6. XPS high resolution scan of Mo 3d and O 1s of LDH with molybdate as the interlayer anion.

Previously, infrared and Raman spectroscopy on the same sample studied here have shown that molybdate anions are not polymerised in the interlayer space of the LDH because of the synthesis under alkaline conditions. The splitting of the vibrational modes of the molybdate anion in the vibrational spectra suggests a symmetry lowering due to interactions of the molybdate anion with the LDH hydroxide surfaces and interlayer water [16]. Palmer, Soisonard and Frost [21] reported a sharp Raman band at around 900 cm^{-1} which was assigned to the MoO_4^{2-} symmetric stretching mode. A single broad IR band at approximately 830 cm^{-1} was reported as characteristic for the MoO_4^{2-} anion, by Klemkaitė-Ramanauskė, *et al.* [76]. Mitchell and Wass [77] confirmed the finding of Adebajo, Musumeci, Kloprogge, Frost and Martens [16] that at pH above 7–8, the prevalent molybdate species was the MoO_4^{2-} ion characterised by an IR band at ca. 830 cm^{-1}, while LDH prepared at pH 4.5 and with high molybdate loadings had an IR band at ca. 920–930 cm^{-1} and bands or shoulders near 890 cm^{-1} suggesting the presence of polymolybdate. Nejati, *et al.* [78] reported a single band in the IR spectrum at 806 cm^{-1} assigned to the antisymmetric stretching mode of Mo–O. Yu, *et al.* [79] observed a similar IR band attritubed to the antisymmetric mode of Mo–O–Mo in MoO_4^{2-} at 834 cm^{-1}. Their Raman spectrum showed the Mo–O symmetrical stretching mode in MoO_4^{2-} at 910 cm^{-1}, while two bands at 320 and 220 cm^{-1} were attributed to the Mo=O bending and Mo–O–Mo deformation mode, respectively. A tetrahedral ion like MoO_4^{2-} has four vibrational modes if it has full Td symmetry. These consist of $\nu_1(A_1)$, $\nu_2(E)$, ν_3, and $\nu_4(F_2)$. The A_1 symmetric stretching mode and the E bending mode are Raman active only, while the F_2 stretching and bending modes are both IR and Raman active. For MoO_4^{2-} the fundamental modes are found at 894 cm^{-1} (ν_1), 381 cm^{-1} (ν_2), 833 cm^{-1} (ν_3), and

 doi:10.20944/preprints202501.0802.v1

318 cm^{-1} (ν_4) [80]. Based on these fundamental modes it seems incorrect to attribute the IR bands at 823 cm^{-1} and 635 cm^{-1} to anti-symmetric and symmetric stretching vibrations of Mo-O bonds as suggested by Colombo, *et al.* [81]. The most complete description has probably been provided by Thao, Trung and Van Long [73]. In the IR spectrum they observed a broad band at 920 cm-1 attributed to the vibrations of Mo=O in polymolybdate $Mo_7O_{24}^{6-}$. A band at 670 cm^{-1} with a shoulder at 856 cm^{-1} was assigned to the Mo–O–Mo stretching mode of MoO42- in the interlayer space of LDH. It is more likely that the 670 cm^{-1} band is associated with NO_3^{-} in the system which is supported by the band at 1370 cm^{-1}. In the Raman spectra, the MoO_4^{2-} symmetric stretching modes in the LDH were observed at 908 and 892 cm^{-1}. They were interpreted as being associated with two different MoO_4^{2-} anionic species, the first one is hydrated and the other one is bonded to the brucite-like hydroxide surface of the LDH within the interlayer space [18]. A broad shoulder at 823 cm^{-1} was ascribed to the MoO_4^{2-} antisymmetric stretching mode, while a band at 325 cm^{-1} was attributed to the Mo-O bending mode [79].

Infrared and Raman spectroscopy have shown that nature of the molybdate anion can change depending on the synthesis conditions, in particular the pH. Under alkaline condition the MoO_4^{2-} anion is dominant, either in a hydrated state or forming a stronger interaction with the hydroxide layer of the LDH within the interlayer space as shown by the slight shift in band positions. Such small changes can not be observed in the XPS spectrum, which only shows that the Mo 3d5/2 peak is found at a slightly lower BE than for molybdate in a rigid crystal structure, indicating that, although there is some interaction with the LDH layer structure, the interaction is not as strong as in molybdate minerals such as wulfenite or other crystalline molybdate compounds [45,51]. In addition, no proof was found for the existence of charge transfer between (Mo^{6+} + O^{2-}) and (Mo^{5+} + O^{-}) as suggested in some papers [74,75].

3.6. Chromate Anion

The Cr 2p high resolution spectrum of the chromate intercalated LDH differs from the other anionic groups shown earlier in this paper in the sense that not one but two Cr 2p3/2 peaks are present (Figure 7 left). The first is a rather broad peak with a BE of 579.0 eV, while the second is much sharper and has a BE of 580.2 eV. The second peak is characteristic for Cr^{6+} in the CrO_4^{2-} anion, while the first peak at lower BE is associated with the presence of Cr^{3+}, indicative of substantial reduction of the CrO_4 with time. Approximately 60 % of all Cr has been reduced based on the peak surface area ratio which is directly proportional to the amounts present. The mineral crocoite $PbCr^{VI}O_4$ showed a Cr 2p3/2 at 579.3 eV [45], while a compound such as $BaCr^{VI}O_4$ has a BE of 579.1 eV. In contrast $Cr^{III}(OH)_3$ has a lower BE of 577.1-577.4 eV [51]. Alidokht, *et al.* [82] observed that upon adsorbtion of chromate using LDH complete reduction of the Cr^{VI} to Cr^{III} took place with Cr 2p3/2 peak at a BE of 277.9 eV. A similar shift was also observed for the reduction of sodium chromate during ion etching in the XPS instrument by Treverton and Davies [83]. The Cr3+ is probably initially present in the form of $Cr(OH)_6^{3-}$ but this anion shows a strong affinity for carbonate [84], so exchange of OH^- for CO_3^{2-} in the anion over time is well possible within the LDH interlayer space given that LDH itself also has a strong affinity for carbonate adsorption. The O 1s peak for the chromate is found around 530.2 eV, which is the same as that of crocoite, $PbCrO_4$ [45], and comparable to compounds such as Na_2CrO_4 at 530.0-530.3 eV, $CaCrO_4$ at 529.5 eV and Li_2CrO_4 at 530.3 eV [51]. The O 1s peak for CrIII compounds occur at slightly high BE and can not be distinguished from the O 1s OH peak of the LDH layer structure (Figure 7 right). The NIST database reports BE values of 530.8 to 531.6 for $Cr(OH)_3$ [51].

 doi:10.20944/preprints202501.0802.v1

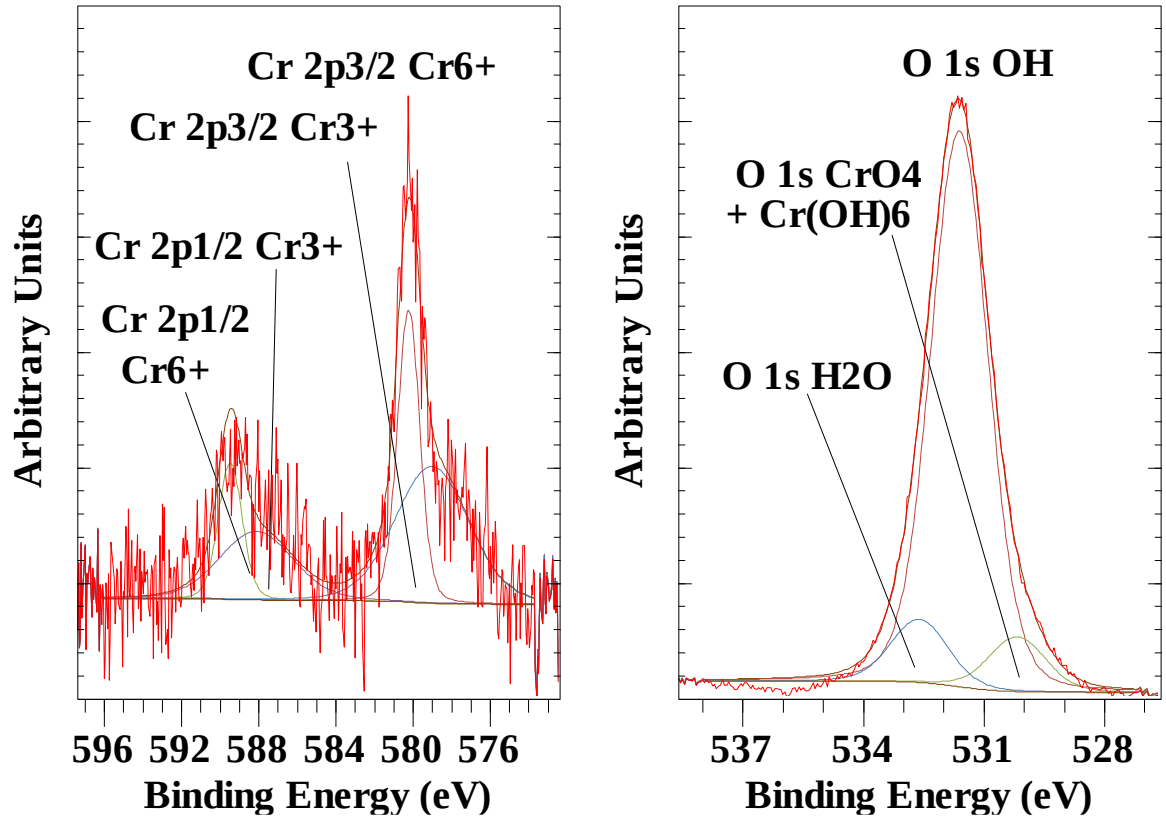

Figure 7. XPS high resolution scan of Cr 2p and O 1s of LDH with chromate as the interlayer anion.

Vibrational spectroscopy (Raman and FTIR) results on the fresh sample showed that the initial chromate anions were not polymerised to $Cr_2O_7^{2-}$ in the LDH interlayer space [16]. The Raman spectrum of the chromate anion in solution reveals distinct vibrational modes: the symmetric stretching mode (ν1) is observed at 848 cm^{-1}, the bending mode (ν2) at 348 cm^{-1}, the asymmetric stretching mode (ν3) at 884 cm^{-1}, and the out-of-plane bending mode (ν4) at 363 cm^{-1}.[80]. Frost, Musumeci, Martens, Adebajo and Bouzaid [18] reported the Raman spectrum of the same freshly prepared sample as later used in this study for the XPS analyses. They observed a strong band at 848 cm^{-1} attributed to the ν_1 symmetric stretching vibrational mode, while two bands at 884 and 928 cm^{-1} were assigned to the ν_3 antisymmetric stretching vibrational mode. The band at 474 cm^{-1} was assigned to the ν_4 bending mode. Finally, two bands at 363 and 237 cm^{-1} were interpreted as being the ν_2 bending modes. The splitting of the ν_3 and ν_2 modes is suggestive of an initial lowering of the symmetry of the chromate anions in the LDH interlayer space prior to partial reduction. The symmetry lowering must be taken into account through the interation of the CrO_4^{2-} anions with both interlayer water and the LDH hydroxide layer surfaces on both sides of the interlayer space. They did not give an explanation for a broad band at 821 cm^{-1}. Although this is lower than reported for fresh $Cr(OH)_3$ around 850 cm^{-1} [85], it is possible that this band is associated with the start of the reduction of the Cr^{6+} to Cr^{3+} and represent the Cr-OH symmetric and antisymmetri stretching mode and the shift is due to the restricted space within the LDH interlayer space. The IR interlayer CrO_4^{2-} υ_3 (Cr-O) mode was reported at 870 cm^{-1} by Del Arco, *et al.* [86]. while Prasanna and Vishnu Kamath [87] found the same band at 866 cm^{-1}. After heating between 100 and 200 ºC, a split of this band was observed and two new bands appared around 874 and 930 cm^{-1} supporting a change in the anion symmetry from T_d to C_{3v} as a result of the interaction between the CrO_4^{2-} and the LDH hydroxide layers similar to what was observed in the Raman spectra by Frost, Musumeci, Martens, Adebajo and Bouzaid [18]. Prasanna, *et al.* [88] also observed in the mid-IR spectrum of intercalated CrO_4^{2-} two bands at 866 and 917 cm^{-1}. The tetrahedral chromate ion is characterized by two distinct IR-active vibrational modes: the antisymmetric stretch (ν_3) and the symmetric deformation mode (ν_4). The ν_4

 doi:10.20944/preprints202501.0802.v1

is expected to be observed around 330 cm^{-1} i.e., outside the mid-IR range and therefore not observed. The two bands represent the triply degenerate (F_2) mode of the chromate. With C_{3v} symmetry the antisymmetric stretching vibration splits into two modes (A_1 + E) [89].

The XPS Cr 2p high resolution scan of the chromate-LDH provided evidence that upon ageing the nature of the interlayer anion changed resulting in the reduction of Cr^{6+} to Cr^{3+}. Since the Raman spectrum of the same sample was taken shortly after synthesis, the spectrum did not show any significant evidence of this reduction [18]. Instead the Raman spectrum is dominated by the CrO_4^{2-} anion with a reduced symmetry, as has also been observed in the infrared spectra of fresh chromate-LDH samples. The XPS data were obtained about 6 months after the Raman spectra and by then approximately 60 % of the Cr^{6+} was reduced to Cr^{3+}.

3.7. Hexacyanoferrate Anions

In earlier work by Kloprogge, Ponce and Ortillo [50] for the hexacyanoferrate(II) anion intercalated in LDH the N 1s peak was found at 397.1 eV for $Fe(CN)_6^{4-}$ while for $Fe(CN)_6^{3-}$ it was observed at 397.4 eV (Figure 8 left). The NIST database shows that $Fe(CN)_6^4$ compounds have N 1s BE values of around 397.4 to 398.0 eV, while $K_3Fe(CN)_6$ had a BE of 398.1 eV [51], indicating that there is a minor difference in BE for N 1s in these two anions.

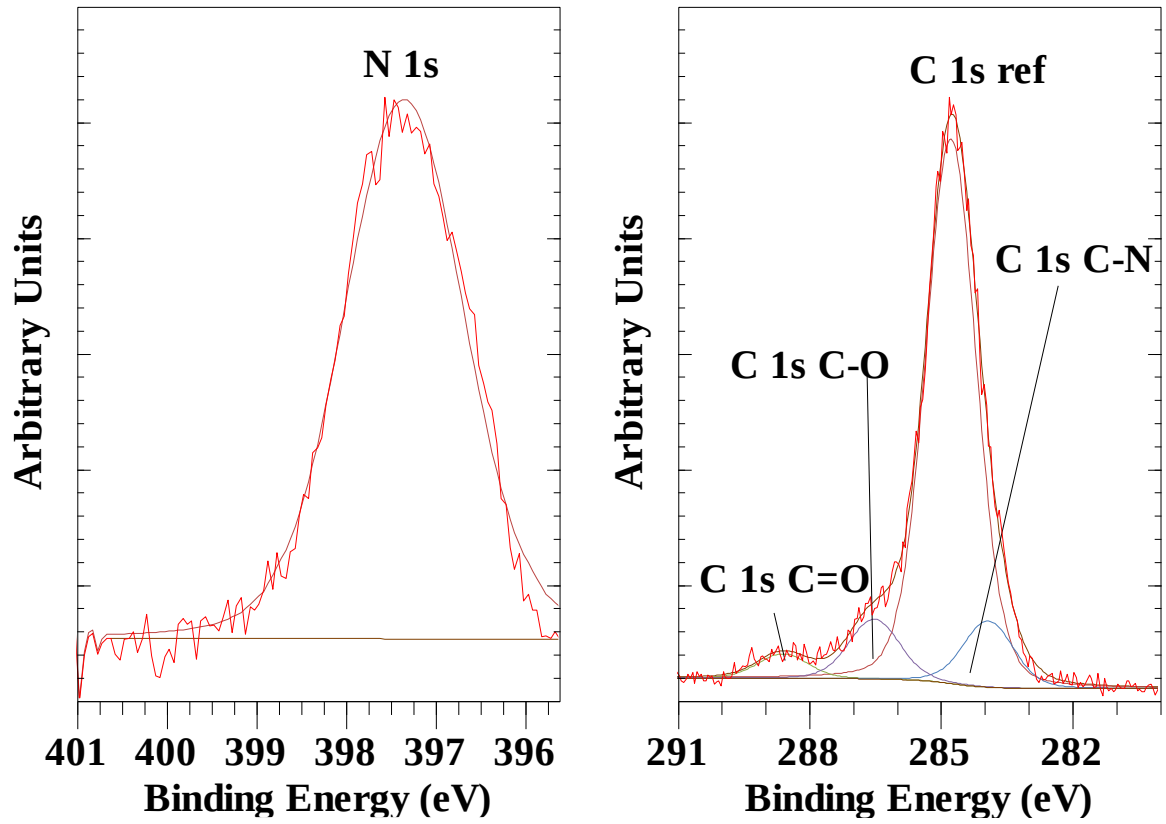

Figure 8. XPS high resolution scan of N 1s and C1s of LDH with $Fe(CN)_6^{4-}$ as the interlayer anion.

There were significant differences in the Fe 2p3/2 high resolution spectra with the $Fe(CN)_6^{3-}$ exhibiting the main peak at a BE of 707.7 eV and a second peak at a BE of 709.5 eV. In contrast, the $Fe(CN)_6^4$ spectrum exhibited only one peak at 707.8 eV (see Figure 14 in [50]). For $K_4Fe(CN)_6$ the NIST database shows a BE value of 707.1 and 708. 5 eV while for $K_3Fe(CN)_6$ it was reported at 709.6 eV [51]. Holgado, *et al.* [90] used Fe-XANES analysis to show that partial reduction of the Fe(III) in the $Fe(CN)_6^4$ intercalated LDH had taken place. Moreover, Idemura, Suzuki and Ono [32] showed the

 doi:10.20944/preprints202501.0802.v1

reduction of Fe(III) in $Fe(CN)_6^{4}$ complexes by Mössbauer spectroscopy. Yamashita and Hayes [91] found that the Fe 2p3/2 for Fe(II) has a BE of about 1 eV lower than Fe(III) in their oxides. The same is true for the potassium hexacyanoferrates and in this study of intercalated LDH with hexacyanoferrates. Kloprogge, Ponce and Ortillo [50] concluded that the Fe 2p3/2 peak at 707.7 eV is due to Fe(II) caused by partial reduction in the initial Fe(III) observed at 709.46 eV. In their study they did not report on the C 1s results for these two samples. For the $Fe(CN)_6^{4-}$LDH the C 1s of the C-N bond was observed at a BE value of 283.5 eV while for $Fe(CN)_6^{3-}$LDH at was observed at 283.9 eV (Figure 8 right). These BE values and the small difference between the two compare well with the values and differences reported for $K_4Fe(CN)_6$ at 283.5 eV and $K_3Fe(CN)_6$ at 283.9 eV [51].

The infrared and Raman spectra of hexacyanoferrate intercalated LDH have been reported for the last 30 years. Kikkawa and Koizumi [92] reported a band around 2000 cm^{-1} assigned to the CN stretching mode. In contrast, Idemura, *et al.* [93] observed for the anion-exchanged LDH in an aqueous solution of $K_3Fe(CN)_6$ resulted in two bands at 2120 and 2040 cm^{-1} in the CN stretching region, indicating that part of the cyanoferrate(III) complex was reduced to cyanoferrate(II) complex during the intercalation. They based this on the fact that pure $K_3Fe(III)(CN)_6$ and $K_4Fe(II)(CN)_6.3H_2O$ produces IR active bands at 2120 and 2040 cm^{-1}, respectively. After the intercalation of $Fe(CN)_6^{4-}$ in the LDH, no change in the oxidation state of Fe was detected. A band at 2040 ± 4 cm^{-1} was the stretching vibration of ν(CN) of $Fe(CN)_6^{4-}$ intercalated in LDH by Mao, *et al.* [94]. Amini, Rahimpour and Jouyban [29] reported two bands at 2038 and 2113 cm^{-1} for $Fe(CN)_6^{3-}$ intercalated Ni/Al–LDH assigned to CN bound to Fe(II) and to CN bound to Fe(III), respectively. Panda, *et al.* [95] described an intense sharp band at 2094 cm^{-1} attributed to the CN stretching mode of hexacyanoferrate(III) anions, but in addition observed two weak bands around 2002 and 2163 cm^{-1}. The band at 2002 cm^{-1} was interpreted as being do to the partial reduction of Fe^{3+} to Fe^{2+}. The weak band at 2163 cm^{-1} was thought to be the result of the formation of nickel ferricyanide, in which the hexacyanoferrate(III) anion is free from the LDH layers. Likewise, Meng, *et al.* [96] observed a band at 2111 cm^{-1} assigned to the CN stretching mode of hexacyanoferrate(III) and a second weak band at 2034 cm^{-1} attributed to the CN stretching mode of hexacyanoferrate(II), suggesting that a small amount of Fe^{3+} was reduced to Fe^{2+} in the LDH interlayer space. Holgado, Rives, Sanromán and Malet [90] described two sharp bands at 2035 ±1 cm^{-1} assigned to CN stretching mode of hexacyanoferrate(II) and at 2120-2086 cm^{-1} attributed to the CN stretching mode of hexacyanoferrate(III) intercalated in LDH.

Hansen and Koch [31] detected the CNstretching mode of hexacyanoferrate(II) and (III) at 2036 and 2112 cm^{-1}, respectively. In addition they observed a band at 2080 cm^{-1}, which they attributed to the presence of free cyanide anions in the interlayer space of the LDH, indicating that the hexacyanoferrate(II,III) cyanide ligands can be replaced with either water or hydroxyls. In addition, oxidation and ligand substitution of the hexacyanoferrate(II) were observed by Mössbauer spectroscopy. In contrast, Yao, *et al.* [97] attributed a band at 2030 cm^{-1} when $Fe(CN)_6^{3-}$ was incorporated in LDH to a CN^- group in which the bond strength of CN^- was weaker due to the interaction with the LDH hydroxide layer. The intensity of the band at 2030 cm^{-1} was shown to increase upon aging. Crespo, *et al.* [98] remarked that regardless of the nature of the starting hexacyanoferrate, two separate or overlapping bands were observed in all cases. Furthermore, the two bands are found closer to each other (maximum $\Delta\nu$ = 46 cm^{-1}) than for the pure potassium salts ($\Delta\nu$ = 73 cm^{-1})indicating that the samples underwent redox processes resulting in a mixture of Fe^{2+} and Fe^{3+} species. They indicated that it is common knowledge from coordination chemistry that the exact band position of the ν(CN) stretching mode for hexacyanoferrate(II) varies with the nature of the countercation. In the case of intercalated LDH hydrogen bonding between interlayer water molecules or the LDH hydroxide layer hydroxyl groups and the cyano groups may likewise have an effect on the exact band position. Fernández, *et al.* [99] observed the most intense band at 2118 cm^{-1}. In addition, a weak band was observed at 2042 cm^{-1}, while even weaker shoulders were detected at 2089 and 2060 cm^{-1}. The ν_{CN} band at 2042 cm^{-1}, indicates a partial Fe^{3+} to Fe^{2+} reduction within the LDH interlayer space similar to other studies. It is known that hexacyanoferrate anions are outer-sphere electron-transfer reductants or oxidants [100,101], based upon which the origin of the two

 doi:10.20944/preprints202501.0802.v1

weaker bands at 2089 and 2060 cm^{-1} can be assigned. Based on Jones [102] the A_{1g}, E_g and T_{1u} ν_{CN} modes required by the O_h point group for $Fe(CN)_6^{4-}$ are found at 2094, 2062 and 2044 cm^{-1} in aqueous solution. The first two modes are infrared-forbidden, but in the restricted interlayer space of the LDH can become partially activated due to a decrease in symmetry, resulting in the two weak bands at 2089 and 2060 cm^{-1}, respectively. If grafting had happened (if the calculated interlayer space height was smaller than the size of the $Fe(CN)_6^{4-}$ anion along the C_3 axis), the decrease in symmetry would be much more dramatic and the infrared spectrum much more complicated. Braterman, *et al.* [103] and Boclair, *et al.* [104] studied oriented samples of hexaxyanoferrate intercalated LDH and compared those to random oriented samples. The random oriented intercalated LDH exhibited two overlapping bands of similar intensity, with the higher wavenumber band being the broader of the two. This higher wavenumber band at 2041 cm^{-1} was still visible in the oriented sample, with unaltered band shape and width, but the sharper, lower wavenumber band at 2035 cm^{-1} was no longer visible. Therefore, both these intense bands were interpreted to correlate with T_{1u} in O_h, and their separation is proof of a local reduction of symmetry. They attributed this effect to a change to D_{3d} symmetry by the ferrocyanide anion, resulting in a splitting of this mode into E_u and A_{2u} components. The symmetry reduction is a result of the orientation of the ferrocyanide anions in the interlayer space of the LDH, which lie with two opposed triangular faces of the coordination octahedron parallel to the internal surfaces of the LDH hydroxide layers. Under these circumstances, the E_u component is likely to be broader than the A_{2u} component. Furthermore, the E_u component is x,y-polarized in the molecular axis system, while the A_{2u} component is z-polarized. This explains the detected selectivity. The molecular three fold z-axis, the crystallographic c axis, and the direction of light propagation are all parallel in the oriented LDH sample.

Two Raman spectroscopic studies on hexacyanoferrate intecalated LDH were published by Kloprogge, *et al.* [105] and Frost, Musumeci, Bouzaid, Adebajo, Martens and Theo Kloprogge [30]. Details about the symmetry of the hexacyanoferrate anion and its reduction and oxidation behavior after intercalation in LDH can be obtained by comparing the Raman spectra with the infrared spectra. Free $Fe(CN)_6^{4-}$ will exhibit three vibrational modes with A_{1g} at 2098 cm^{-1} and E_g at 2062 cm^{-1} in the Raman spectrum and T_{1u} at 2044 cm^{-1} in the infrared spectrum. For the intercalated LDH, they detected bands in the Raman spectrum at 2136, 2094 and 2065 cm^{-1} for hexacyanoferrate(II) intercalated LDH, and at 2164, 2136, 2094 and 2059 cm^{-1} for hexacyanferrate(III) intercalated LDH, clearly supporting the fact that a change in the site symmetry had taken place as well as partial reduction. Lowering of the site symmetry to C_3 after intercalation in LDH would predict four bands in the Raman spectra for both the hexacyanoferrate (II) and hexacyanoferrate(III) anions resulting in theoretically eight modes. In reality, it is to be expected that a number of these modes will overlap causing the detection of fewer bands.

It is clear in the case of hexacyanoferrate(III) intercalation in LDH generally results in a partial reduction of Fe3+ to Fe2+. In contrast to the other anionic groups studied here, the reduction of hexacyanoferrate(III) results in clear changes in the infrared and Raman spectra. These changes are also clearly visible in the XPS Fe 2p spectra. Integration of the peak areas for both the Fe 2p3/2 of Fe(II) and Fe(III) allows for a direct measure of the amount of reduction. In this sample 45 % of the Fe(III) has been reduced to Fe(II).

3.8. Influence of Interlayer Anions on the LDH Layer Structure

From the previous sections it is clear that the nature of the interlayer anion can be studied not only by vibrational spectroscopy (infrared and Raman) but also by XPS and additional information can be obtained. In most instances the BE of the non-oxygen atom is slighly lower compared to minerals in which the anion forms part of the rigid crystal crystal structure. In several instances evidence was found for partial reduction of the metal upon intercalation, which was not detected by vibrational spectroscopy. Since the interlayer anions are interaction, most likely through hydrogen bonds with the hydroxide layers of the LDH within the interlayer space, it is of interest to see if the atoms that make up the LDH layer structure are in any way affected by the nature of the interlayer

 doi:10.20944/preprints202501.0802.v1

anion. Table 1 provides an overview of the BE values obtained for Al 2p, Mg 2p and O 1s for the hydroxyl group. In all instances the BE values are very close though it seems that the MoO_4^{2-} and CrO_4^{2-} ions with their much heavier metals result in slightly lower BE values for Al 2p, Mg 2p and O 1s. The differences, however, are so small that they may be considered to be within the experimental error of XPS.

Table 1. BE values of Al 2p, Mg 2p and O 1s for the LDH layer structure as function of the interlayer anion.

Anion	Al 2p	Mg 2p	O 1s OH
CO_3^{2-}	74.5	50.1	531.6
PO_4^{3-} pH 11.9	74.4	50.1	531.7
PO_4^{3-} pH 12.5	74.5	50.1	531.7
SO_4^{2-}	74.3	49.9	531.7
MoO_4^{2-}	74.2	49.8	531.5
CrO_4^{2-}	74.3	49.9	531.6
$Fe(CN)_6^{4-}$	74.4	50.0	531.7
$Fe(CN)_6^{3-}$	74.4	50.0	531.7

5. Conclusions

This comprehensive analysis of Layered Double Hydroxides (LDHs) intercalated with various anionic species elucidates the intricate interplay between interlayer anions and LDH structural dynamics. X-ray photoelectron spectroscopy (XPS) characterized the distinct binding energies for key elements, confirming the presence of carbonate, phosphate, sulfate, molybdate, chromate, and hexacyanoferrate anions within the interlayer space. The carbonate anion exhibited a notable reduction in binding energy compared to common carbonate minerals, attributed to interactions with interlayer water and hydroxyl groups, suggesting semi-constrained behavior within the LDH framework. In contrast, phosphate intercalation demonstrated stability without shifts in binding energies, while sulfate ions indicated limited movement, suggesting moderate interaction with hydroxide layers. Molybdate displayed weaker interactions than crystalline counterparts, reflecting the influence of LDH synthesis conditions. A significant observation was the reduction of chromate ions from Cr^{6+} to Cr^{3+}, indicating dynamic redox behavior within the interlayer space. Furthermore, hexacyanoferrate anions revealed partial reduction, with distinctive spectral differences indicating site symmetry alterations. Collectively, these findings articulate the necessity for considering anion identity and synthesis parameters in the application and functional design of LDHs, highlighting their potential roles in catalysis, ion exchange, and environmental remediation. Further investigations into the relationships between interlayer anions and LDH stability are warranted to broaden the understanding of their reactivity and utility in advanced materials science.

Author Contributions: Conceptualization, J.T.K.; methodology, J.T.K.; validation, J.T.K.; formal analysis, J.T.K; investigation, J.T.K.; resources, J.T.K.; data curation, J.T.K.; writing—original draft preparation, J.T.K; writing—review and editing, J.T.K.; visualization, J.T.K.;; project administration, X.X J.T.K.; funding acquisition, J.T.K. All authors have read and agreed to the published version of the manuscript.

Funding: This research received no external funding.

Data Availability Statement: Not applicable.

Acknowledgments: The author acknowledges the facilities and the scientific and technical assistance of the Australian Microscopy & Microanalysis Research Facility at the Centre for Microscopy and Microanalysis, The University of Queensland. The authors also acknowledge the provision of library resources and access to journals by the University of the Philippines System

Conflicts of Interest: The author declares no conflicts of interest.

References

1. Mishra, G.; Dash, B.; Pandey, S. Layered double hydroxides: A brief review from fundamentals to application as evolving biomaterials. *Applied Clay Science* **2018**, *153*, 172-186, doi:https://doi.org/10.1016/j.clay.2017.12.021.
2. Evans, D.G.; Slade, R.C.T. Structural Aspects of Layered Double Hydroxides. In *Layered Double Hydroxides*, Duan, X., Evans, D.G., Eds.; Springer Berlin Heidelberg: Berlin, Heidelberg, 2006; pp. 1-87.
3. Wypych, F.; de Freitas, R.A. Chapter 10 - Layered double hydroxides and hydroxide salts: Structure and properties. In *Developments in Clay Science*, Wypych, F., de Freitas, R.A., Eds.; Elsevier: 2022; Volume 10, pp. 317-350.
4. Miyata, S.; Kumura, T. Synthesis of new hydrotalcite-like compounds and their physico-chemical properties *Chem.Letters* **1973**, 843–848, doi:https://doi.org/10.1246/cl.1973.843.
5. Vaccari, A. Preparation and Catalytic properties of cationic and anionic clays. *Catal. Today* **1998**, *41*, 53–71, doi:https://doi.org/10.1016/S0920-5861(98)00038-8.
6. Farhan, A.; Khalid, A.; Maqsood, N.; Iftekhar, S.; Sharif, H.M.A.; Qi, F.; Sillanpää, M.; Asif, M.B. Progress in layered double hydroxides (LDHs): Synthesis and application in adsorption, catalysis and photoreduction. *Science of The Total Environment* **2024**, *912*, 169160, doi:https://doi.org/10.1016/j.scitotenv.2023.169160.
7. Kameliya, J.; Verma, A.; Dutta, P.; Arora, C.; Vyas, S.; Varma, R.S. Layered Double Hydroxide Materials: A Review on Their Preparation, Characterization, and Applications. *Inorganics* **2023**, *11*, 121, doi:https://doi.org/10.3390/inorganics11030121.
8. Karmakar, A.K.; Hasan, M.S.; Sreemani, A.; Das Jayanta, A.; Hasan, M.M.; Tithe, N.A.; Biswas, P. A review on the current progress of layered double hydroxide application in biomedical sectors. *The European Physical Journal Plus* **2022**, *137*, 801, doi:https://doi.org/10.1140/epjp/s13360-022-02993-0.
9. Tang, S.; Yao, Y.; Chen, T.; Kong, D.; Shen, W.; Lee, H.K. Recent advances in the application of layered double hydroxides in analytical chemistry: A review. *Analytica Chimica Acta* **2020**, *1103*, 32-48, doi:https://doi.org/10.1016/j.aca.2019.12.065.
10. Wang, P.; Zhang, X.; Zhou, B.; Meng, F.; Wang, Y.; Wen, G. Recent advance of layered double hydroxides materials: Structure, properties, synthesis, modification and applications of wastewater treatment. *Journal of Environmental Chemical Engineering* **2023**, *11*, 111191, doi:https://doi.org/10.1016/j.jece.2023.111191.
11. Nalawade, P.; Aware, B.N.; Kadam, V.J.; Hirlekar, R.S. Layered double hydroxides: A review. *Journal of Scientific & Industrial Research* **2009**, *68*, 267-272.
12. Evana, E.; Marchidan, R.; Mănăila, R. NO_3^- - CO_3^{2-} anion exchange during washing of Ni-Al hydroxy-compounds. *Bull.Soc. Chim. Belge* **1992**, *2*, 101–107, doi:https://doi.org/10.1002/bscb.19921010204.
13. Miyata, S. The synthesis of hydrotalcite-like compounds and their structures and physico-chemical properties - I: the systems Mg^{2+}-Al^{3+}-NO_3^-, Mg^{2+}-A^{l3+}-Cl^-, Mg^{2+}-Al^{3+}-ClO_4^-, Ni^{2+}-Al^{3+}-Cl^- and Zn^{2+}-Al^{3+}-Cl^-. *Clays Clay Miner.* **1975**, *23*, 369–375, doi:https://doi.org/10.1346/CCMN.1975.0230508.
14. Miyata, S.; Okada, A. Synthesis of hydrotalcite-like compounds and their physico-chemical properties – the system Mg^{2+} - Al^{3+} - SO_4^{2-} and Mg^{2+} - Al^{3+} - CrO_4^{2-}. *Clays Clay Miner.* **1977**, *25*, 14–18, doi:https://doi.org/10.1346/CCMN.1977.0250103.
15. Reichle, W.T.; Kang, S.Y.; Everhardt, D.S. The nature of the thermal decomposition of a catalytically active anionic clay mineral. *J. Catalysis* **1986**, *101*, 352–359, doi:https://doi.org/10.1016/0021-9517(86)90262-9.
16. Adebajo, M.O.; Musumeci, A.W.; Kloprogge, J.T.; Frost, R.L.; Martens, W.N. Synthesis and characterization of hydrotalcites containing interlayer sulphate, molybdate and chromate anions. In Proceedings of the 13th International Clay Conference, August 21-27, 2005, Tokyo, Japan, 2005; p. 127.
17. Frost, R.L.; Musumeci, A.W.; Kloprogge, J.T.; Adebajo, M.O.; Martens, W.N. Raman spectroscopy of hydrotalcites with phosphate in the interlayer: implications for the removal of phosphate from water. *J. Raman Spectrosc.* **2006**, *37*, 733-741, doi:https://doi.org/10.1002/jrs.1500.

18. Frost, R.L.; Musumeci, A.W.; Martens, W.N.; Adebajo, M.O.; Bouzaid, J. Raman spectroscopy of hydrotalcites with sulphate, molybdate and chromate in the interlayer. *J. Raman Spectrosc.* **2005**, *36*, 925-931, doi:https://doi.org/10.1002/jrs.1385.
19. Kloprogge, J.T.; Wharton, D.; Hickley, L.; Frost, R.L. Infrared and Raman study of interlayer anions CO_3^{2-}, NO_3^-, SO_4^{2-} and ClO_4^- in Mg/Al-hydrotalcite. *Amer. Miner.* **2002**, *87*, 623-629, doi:https://doi.org/10.2138/am-2002-5-604.
20. Ookubo, A.; Ooi, K.; Tani, F.; Hayashi, H. Phase Transition of Cl--Intercalated Hydrotalcite-like Compound during Ion Exchange with Phosphates. *Langmuir* **1994**, *10*, 407-411, doi:https://doi.org/10.1021/la00014a013.
21. Palmer, S.J.; Soisonard, A.; Frost, R.L. Determination of the mechanism(s) for the inclusion of arsenate, vanadate, or molybdate anions into hydrotalcites with variable cationic ratio. *J. Colloid Interface Sci.* **2009**, *329*, 404-409, doi:https://doi.org/10.1016/j.jcis.2008.09.065.
22. Wang, X.; Cai, Y.; Han, T.; Fang, M.; Chen, K.; Tan, X. Phosphate functionalized layered double hydroxides (phos-LDH) for ultrafast and efficient U(VI) uptake from polluted solutions. *J. Hazard. Mater.* **2020**, *399*, 123081, doi:https://doi.org/10.1016/j.jhazmat.2020.123081.
23. Pálinkó, I.; Sipos, P.; Berkesi, O.; Varga, G. Distinguishing Anionic Species That Are Intercalated in Layered Double Hydroxides from Those Bound to Their Surface: A Comparative IR Study. *The Journal of Physical Chemistry C* **2022**, *126*, 15254-15262, doi:https://doi.org/10.1021/acs.jpcc.2c03547.
24. Radha, S.; Vishnu Kamath, P. Electronic spectra of anions intercalated in layered double hydroxides. *Bulletin of Materials Science* **2013**, *36*, 923-929, doi:https://doi.org/10.1007/s12034-013-0538-0.
25. Mora, M.; Jiménez-Sanchidrián, C.; Rafael Ruiz, J. Raman spectroscopy study of layered-double hydroxides containing magnesium and trivalent metals. *Materials Letters* **2014**, *120*, 193-195, doi:https://doi.org/10.1016/j.matlet.2014.01.085.
26. Lv, S.; Zhao, Y.; Zhang, L.; Zhang, T.; Dong, G.; Li, D.; Cheng, S.; Ma, S.; Song, S.; Quintana, M. Anion regulation strategy of lithium-aluminum layered double hydroxides for strengthening resistance to deactivation in lithium recovery from brines. *Chemical Engineering Journal* **2023**, *472*, 145026, doi:https://doi.org/10.1016/j.cej.2023.145026.
27. Ciocan, C.E.; Dumitriu, E.; Cacciaguerra, T.; Fajula, F.; Hulea, V. New approach for synthesis of Mo-containing LDH based catalysts. *Catalysis Today* **2012**, *198*, 239-245, doi:https://doi.org/10.1016/j.cattod.2012.04.071.
28. Schutz, A.; Biloen, P. Interlamellar chemistry of hydrotalcites. I. Polymerzation of silcate anions. *J. Solid State Chem.* **1987**, *68*, 360–368, doi:https://doi.org/10.1016/0022-4596(87)90323-9.
29. Amini, R.; Rahimpour, E.; Jouyban, A. An optical sensing platform based on hexacyanoferrate intercalated layered double hydroxide nanozyme for determination of chromium in water. *Anal. Chim. Acta* **2020**, *1117*, 9-17, doi:https://doi.org/10.1016/j.aca.2020.04.001.
30. Frost, R.L.; Musumeci, A.W.; Bouzaid, J.; Adebajo, M.O.; Martens, W.N.; Theo Kloprogge, J. Intercalation of hydrotalcites with hexacyanoferrate(II) and (III)—a thermoRaman spectroscopic study. *J. Solid State Chem.* **2005**, *178*, 1940-1948, doi:https://doi.org/10.1016/j.jssc.2005.03.045.
31. Hansen, H.C.B.; Koch, C.B. Synthesis and Properties of Hexacyanoferrate Interlayered in Hydrotalcite. I. Hexacyanoferrate(II). *Clays Clay Miner.* **1994**, *42*, 170-179, doi:https://doi.org/10.1346/CCMN.1994.0420207.
32. Idemura, S.; Suzuki, E.; Ono, Y. Electronic State of Iron Complexes in the Interlayer of Hydrotalcite-Like Materials. *Clays Clay Miner.* **1989**, *37*, 553–557, doi:https://doi.org/10.1346/CCMN.1989.0370608.
33. Wang, J.; Tian, Y.; Wang, R.C.; Colon, J.L.; Cearfield, A. Systematic preparation of polyoxometalate pillared layered double hydroxides via direct aqueous reaction. *Mater. Res. Soc. Symp. Proc.* **1991**, *233*, 63–80, doi:https://doi.org/10.1557/PROC-233-63.
34. Carpani, I.; Berrettoni, M.; Ballarin, B.; Giorgetti, M.; Scavetta, E.; Tonelli, D. Study on the intercalation of hexacyanoferrate(II) in a Ni, Al based hydrotalcite. *Solid State Ionics* **2004**, *168*, 167-175, doi:https://doi.org/10.1016/j.ssi.2004.01.032.
35. Crespo, I.; Barriga, C.; Rives, V.; Ulibarri, M.A. Intercalation of iron hexacyano complexes in zn,al-hydrotalcite. *Solid State Ionics* **1997**, *101-103*, 729-735, doi:https://doi.org/10.1016/S0167-2738(97)00290-7.

36. Zhang, T.; Zhao, B.; Chen, Q.; Peng, X.; Yang, D.; Qiu, F. Layered double hydroxide functionalized biomass carbon fiber for highly efficient and recyclable fluoride adsorption. *Applied Biological Chemistry* **2019**, *62*, 12, doi:https://doi.org/10.1186/s13765-019-0410-z.
37. Bao, W.; Tang, Y.; Yu, J.; Yan, W.; Wang, C.; Li, Y.; Wang, Z.; Yang, J.; Zhang, L.; Yu, F. Si-doped ZnAl-LDH nanosheets by layer-engineering for efficient photoelectrocatalytic water splitting. *Applied Catalysis B: Environment and Energy* **2024**, *346*, 123706, doi:https://doi.org/10.1016/j.apcatb.2024.123706.
38. Lv, H.; Rao, H.; Liu, Z.; Zhou, Z.; Zhao, Y.; Wei, H.; Chen, Z. NiAl layered double hydroxides with enhanced interlayer spacing via ion-exchange as ultra-high performance supercapacitors electrode materials. *Journal of Energy Storage* **2022**, *52*, 104940, doi:https://doi.org/10.1016/j.est.2022.104940.
39. Li, R.; Xu, J.; Pan, Q.; Ba, J.; Tang, T.; Luo, W. One-Step Synthesis of NiFe Layered Double Hydroxide Nanosheet Array/N-Doped Graphite Foam Electrodes for Oxygen Evolution Reactions. *ChemistryOpen* **2019**, *8*, 1027-1032, doi:https://doi.org/10.1002/open.201900190.
40. Mahmoud, R.K.; Taha, M.; Zaher, A.; Amin, R.M. Understanding the physicochemical properties of Zn–Fe LDH nanostructure as sorbent material for removing of anionic and cationic dyes mixture. *Scientific Reports* **2021**, *11*, 21365, doi:https://doi.org/10.1038/s41598-021-00437-w.
41. Li, X.; Fortunato, M.; Cardinale, A.M.; Sarapulova, A.; Njel, C.; Dsoke, S. Electrochemical study on nickel aluminum layered double hydroxides as high-performance electrode material for lithium-ion batteries based on sodium alginate binder. *Journal of Solid State Electrochemistry* **2022**, *26*, 49-61, doi:https://doi.org/10.1007/s10008-021-05011-y.
42. Shen, W.; Hu, T.; Liu, X.; Zha, J.; Meng, F.; Wu, Z.; Cui, Z.; Yang, Y.; Li, H.; Zhang, Q.; et al. Defect engineering of layered double hydroxide nanosheets as inorganic photosensitizers for NIR-III photodynamic cancer therapy. *Nature Communications* **2022**, *13*, 3384, doi:https://doi.org/10.1038/s41467-022-31106-9.
43. Kloprogge, J.T.; Frost, R.L. Fourier Transform Infrared and Raman spectroscopic study of the local structure of Mg, Ni and Co — hydrotalcites. *J.Solid State Chem.* **1999**, *146*, 506–515, doi:https://doi.org/10.1006/jssc.1999.8413.
44. Frost, R.L.; Musumeci, A.W.; Kloprogge, J.T.; Weier, M.; Adebajo, M.; Martens, W.N. Thermal decomposition of hydrotalcite with hexacyanoferrate(II) and hexacyanoferrate(III) anions in the interlayer. *J. Therm. Anal. Cal.* **2006**, *86*, 205-209, doi:https://doi.org/10.1007/s10973-005-6933-z.
45. Kloprogge, J.T.; Wood, B.J. *Handbook of Mineral Spectroscopy Volume 1 X-ray Photoelectron Spectra*; Elsevier: Amsterdam, 2020; Volume 1, p. 505.
46. Kloprogge, J.T.; Duong, L.V.; Wood, B.J.; Frost, R.L. XPS study of the major minerals in bauxite: Gibbsite, bayerite and (pseudo-)boehmite. *J. Colloid Interface Sci.* **2006**, *296*, 572–576, doi:https://doi.org/10.1016/j.jcis.2005.09.054.
47. Peng, C.; Yu, J.; Zhao, Z.; Dai, J.; Fu, J.; Zhao, M.; Wang, W. Synthesis and Properties of a Clean and Sustainable Deicing Additive for Asphalt Mixture. *PLoS ONE* **2015**, *10*, e0115721, doi:https://doi.org/10.1371/journal.pone.0115721.
48. Rey, F.; Fornes, V.; Rojo, J.M. Thermal decomposition of hydrotalcites. An infrared and nuclear magnetic resonance spectroscopic study. *J. Chem. Soc., Faraday Trans.*, **1992**, *88*, 2233–2238, doi:https://doi.org/10.1039/FT9928802233.
49. Alzamora, L.E.; Ross, J.R.; Kruissink, E.C.; Reijen, L.L.v. Coprecipitated Nickel-Alumina catalysts for methanation at high temperature. *J. Chem. Soc., Faraday Trans. I* **1981**, *77*, 665–681, doi:https://doi.org/10.1039/F19817700665.
50. Kloprogge, J.T.; Ponce, C.P.; Ortillo, D.O. X-ray Photoelectron Spectroscopic Study of Some Organic and Inorganic Modified Clay Minerals. *Materials* **2021**, *14*, 7115, doi:https://doi.org/10.3390/ma14237115.
51. Naumkin, A., V; Kraut-Vass, A.; Gaarenstroom, S.W.; C.J., P. NIST X-ray Photoelectron Spectroscopy Database, NIST Standard Reference Database Number 20. Available online: https://srdata.nist.gov/xps/Default.aspx (accessed on 29 November).
52. Gupta, N.K.; Saifuddin, M.; Kim, S.; Kim, K.S. Microscopic, spectroscopic, and experimental approach towards understanding the phosphate adsorption onto Zn–Fe layered double hydroxide. *J. Mol. Liquids* **2020**, *297*, 111935, doi:https://doi.org/10.1016/j.molliq.2019.111935.

53. Benício, L.P.F.; Constantino, V.R.L.; Pinto, F.G.; Vergütz, L.; Tronto, J.; Da Costa, L.M. Layered Double Hydroxides: New Technology in Phosphate Fertilizers Based on Nanostructured Materials. *ACS Sustain. Chem. Eng.* **2017**, *5*, 399–409, doi:10.1021/acssuschemeng.6b01784.
54. Benício, L.P.F.; Eulálio, D.; Guimarães, L.D.M.; Pinto, F.G.; Costa, L.M.D.; Tronto, J. Layered Double Hydroxides as Hosting Matrices for Storage and Slow Release of Phosphate Analyzed by Stirred-Flow Method. *Mater. Res.* **2018**, *21*, e20171004, doi:https://doi.org/10.1590/1980-5373-MR-2017-1004.
55. Yang, K.; Yan, L.-g.; Yang, Y.-m.; Yu, S.-j.; Shan, R.-r.; Yu, H.-q.; Zhu, B.-c.; Du, B. Adsorptive removal of phosphate by Mg–Al and Zn–Al layered double hydroxides: Kinetics, isotherms and mechanisms. *Sep. Pur. Techn.* **2014**, *124*, 36-42, doi:https://doi.org/10.1016/j.seppur.2013.12.042.
56. Ross, S.D. Phosphates and other Oxy-anions of Group V. In *The Infrared Spectra of Minerals*, Farmer, V.C., Ed.; Mineralogical Society of Great Britain and Ireland: 1974; Volume 4, pp. 383-422.
57. Miller, F.A.; Wilkins, C.H. Infrared Spectra and Characteristic Frequencies of Inorganic Ions. *Anal. Chem.* **1952**, *24*, 1253-1294, doi:https://doi.org/10.1021/ac60068a007.
58. Shabanian, M.; Hajibeygi, M.; Raeisi, A. 2 - FTIR characterization of layered double hydroxides and modified layered double hydroxides. In *Layered Double Hydroxide Polymer Nanocomposites*, Thomas, S., Daniel, S., Eds.; Woodhead Publishing: 2020; pp. 77-101.
59. Cheng, X.; Huang, X.; Wang, X.; Sun, D. Influence of calcination on the adsorptive removal of phosphate by Zn–Al layered double hydroxides from excess sludge liquor. *J. Hazard. Mater.* **2010**, *177*, 516-523, doi:https://doi.org/10.1016/j.jhazmat.2009.12.063.
60. He, H.; Kang, H.; Ma, S.; Bai, Y.; Yang, X. High adsorption selectivity of ZnAl layered double hydroxides and the calcined materials toward phosphate. *J. Colloid Interf. Sci.* **2010**, *343*, 225-231, doi:https://doi.org/10.1016/j.jcis.2009.11.004.
61. Bish, D.L.; Livingstone, A. The crystal chemistry and paragenesis of honessite and hydrohonessite: the sulfate analogues of reevesite. *Miner. Mag.* **1981**, *44*, 339–343, doi:https://doi.org/10.1180/minmag.1981.044.335.15.
62. Nickel, E.H.; Clarke, R.M. Carrboydite, a hydrated sulfate of nickel and aluminum: a new mineral from Western Australia. *Amer. Miner.* **1976**, *61*, 366–372.
63. Nickel, E.H.; Wildman, J.E. Hydrohonessite- a new hydrated Ni-Fe hydroxy-sulphate mineral; its relationship to honessite, carrboydite, and minerals of the pyroaurite group. *Miner. Mag.* **1981**, *44*, 333-337, doi:https://doi.org/10.1180/minmag.1981.044.335.14.
64. Wahlqvist, M.; Shchukarev, A. XPS spectra and electronic structure of Group IA sulfates. *J. Electr. Spectros. Rel. Phenom.* **2007**, *156-158*, 310-314, doi:https://doi.org/10.1016/j.elspec.2006.11.032.
65. Ross, S.D. *Inorganic Infrared and Raman Spectra*; McGraw-Hill Book Company: London, 1972; p. 140.
66. Kloprogge, J.T.; Hickey, L.; Frost, R.L. Synthesis and spectroscopic characterization of deuterated hydrotalcite. *J. Mater. Sci. Letters* **2001**, *21*, 603-605, doi:https://doi.org/10.1023/A:1015655018529.
67. Fahami, A.; Beall, G.W. Mechanosynthesis and characterization of Hydrotalcite like Mg–Al–SO_4-LDH. *Mater. Letters* **2016**, *165*, 192-195, doi:https://doi.org/10.1016/j.matlet.2015.11.132.
68. Liu, Y.; Yang, Z. Intercalation of sulfate anions into a Zn–Al layered double hydroxide: their synthesis and application in Zn–Ni secondary batteries. *RSC Advanc.* **2016**, *6*, 68584-68591, doi:10.1039/C6RA09096F.
69. Frost, R.L.; Theiss, F.L.; López, A.; Scholz, R. Vibrational spectroscopic study of the sulphate mineral glaucocerinite $(Zn,Cu)_{10}Al_6(SO_4)_3(OH)_{32}\cdot 18H_2O$ – A natural layered double hydroxide. *Spectrochim. Acta A: Mol. Biomol. Spectrosc.* **2014.** , *127*, 349–354, doi:https://doi.org/10.1016/j.saa.2014.02.086.
70. Dutta, P.K.; Puri, M. Anion exchange in lithium aluminate hydroxides. *J. Phys. Chem.* **1989**, *93*, 376–381, doi:https://doi.org/10.1021/j100338a072.
71. Bish, D.L. Anion-exchange in takovite: applications to other hydroxide minerals. *Bull. Miner.* **1980**, *103*, 170–175, doi:https://doi.org/10.3406/bulmi.1980.7392.
72. Lin, Y.-H.; Adebajo, M.O.; Kloprogge, J.T.; Martens, W.N.; Frost, R.L. X-ray diffraction and Raman spectroscopic studies of Zn-substituted carrboydite-like compounds. *Mater. Chem. Phys.* **2006**, *100*, 174-186, doi:https://doi.org/10.1016/j.matchemphys.2005.12.028.

73. Thao, N.T.; Trung, N.D.; Van Long, D. Activity of Molybdate-Intercalated Layered Double Hydroxides in the Oxidation of Styrene with Air. *Catal. Letters* **2016**, *146*, 918-928, doi:https://doi.org/10.1007/s10562-016-1710-0.
74. Behera, G.C.; Parida, K.M. A comparative study of molybdenum promoted vanadium phosphate catalysts towards epoxidation of cyclohexene. *Appl. Catal. A: General* **2013**, *464-465*, 364-373, doi:https://doi.org/10.1016/j.apcata.2013.06.012.
75. Baltrusaitis, J.; Mendoza-Sanchez, B.; Fernandez, V.; Veenstra, R.; Dukstiene, N.; Roberts, A.; Fairley, N. Generalized molybdenum oxide surface chemical state XPS determination via informed amorphous sample model. *Appl. Surf. Sci.* **2015**, *326*, 151-161, doi:https://doi.org/10.1016/j.apsusc.2014.11.077.
76. Klemkaitė-Ramanauskė, K.; Žilinskas, A.; Taraškevičius, R.; Khinsky, A.; Kareiva, A. Preparation of Mg/Al layered double hydroxide (LDH) with structurally embedded molybdate ions and application as a catalyst for the synthesis of 2-adamantylidene(phenyl)amine Schiff base. *Polyhedron* **2014**, *68*, 340-345, doi:https://doi.org/10.1016/j.poly.2013.11.009.
77. Mitchell, P.C.H.; Wass, S.A. Propane dehydrogenation over molybdenum hydrotalcite catalysts. *Appl. Catal. A: General* **2002**, *225*, 153-165, doi:https://doi.org/10.1016/S0926-860X(01)00862-6.
78. Nejati, K.; Akbari, A.R.; Davari, S.; Asadpour-Zeynali, K.; Rezvani, Z. Zn–Fe-layered double hydroxide intercalated with vanadate and molybdate anions for electrocatalytic water oxidation. *New J. Chem.* **2018**, *42*, 2889-2895, doi:10.1039/C7NJ04469K.
79. Yu, X.; Wang, J.; Zhang, M.; Yang, P.; Yang, L.; Cao, D.; Li, J. One-step synthesis of lamellar molybdate pillared hydrotalcite and its application for AZ31 Mg alloy protection. *Solid State Sci.* **2009**, *11*, 376-381, doi:https://doi.org/10.1016/j.solidstatesciences.2008.08.003.
80. Ross, S.D. Sulphates and other Oxy-anions of Group VI. In *The Infrared Spectra of Minerals*, Farmer, V.C., Ed.; Mineralogical Society of Great Britain and Ireland: London, 1974; Volume 4, pp. 423-444.
81. Colombo, K.; Maruyama, S.; Yamamoto, C.; Wypych, F. Intercalation of Molybdate Ions into Ni/Zn Layered Double Hydroxide Salts: Synthesis, Characterization, and Preliminary Catalytic Activity in Methyl Transesterification of Soybean Oil. *J. Brazil. Chem. Soc.* **2016**, *28*, 1315-1322, doi:https://doi.org/10.21577/0103-5053.20160298.
82. Alidokht, L.; Oustan, S.; Khataee, A.; Neyshabouri, M.; Reyhanitabar, A. Removal of chromate from aqueous solution by reduction with nanoscale Fe–Al layered double hydroxide. *Res. Chem. Intermed.* **2018**, *44*, 2319-2331, doi:10.1007/s11164-017-3231-x.
83. Treverton, J.A.; Davies, N.C. An XPS study of chromate pretreatment of aluminium. *Metals Techn.* **1977**, *4*, 480-489, doi:https://doi.org/10.1179/030716977803292808.
84. Amonette, J.E.; Rai, D. Identification of Noncrystalline (Fe,Cr)(OH)$_3$ by Infrared Spectroscopy. *Clays Clay Miner.* **1990**, *38*, 129-136, doi:10.1346/CCMN.1990.0380203.
85. Gomes, A.S.O.; Yaghini, N.; Martinelli, A.; Ahlberg, E. A micro-Raman spectroscopic study of Cr(OH)$_3$ and Cr_2O_3 nanoparticles obtained by the hydrothermal method. *J. Raman Spectrosc.* **2017**, *48*, 1256–1263, doi:https://doi.org/10.1002/jrs.5198.
86. Del Arco, M.; Carriazo, D.; Martín, C.; Pérez Grueso, A.M.; Rives, V. Characterization of Chromate-Intercalated Layered Double Hydroxides. *Mater. Sci. Forum* **2006**, *514-516*, 1541–1545, doi:https://doi.org/10.4028/www.scientific.net/MSF.514-516.1541.
87. Prasanna, S.V.; Vishnu Kamath, P. Chromate uptake characteristics of the pristine layered double hydroxides of Mg with Al. *Solid State Sci.* **2008**, *10*, 260-266, doi:https://doi.org/10.1016/j.solidstatesciences.2007.09.023.
88. Prasanna, S.V.; Rao, R.A.P.; Kamath, P.V. Layered double hydroxides as potential chromate scavengers. *J. Colloid Interf. Sci.* **2006**, *304*, 292-299, doi:https://doi.org/10.1016/j.jcis.2006.08.064.
89. Ross, S.D. *Inorganic infrared and Raman spectra*; McGraw-Hill: London, 1972; p. 414.
90. Holgado, M.J.; Rives, V.; Sanromán, M.S.; Malet, P. Hexacyanoferrate-interlayered hydrotalcite. *Solid State Ion.* **1996**, *92*, 273–283, doi:https://doi.org/10.1016/S0167-2738(96)00478-X.
91. Yamashita, T.; Hayes, P. Analysis of XPS spectra of Fe^{2+} and Fe^{3+} ions in oxide materials. *Appl. Surf. Sci.* **2008**, *254*, 2441–2449, doi:https://doi.org/10.1016/j.apsusc.2007.09.063.

92. Kikkawa, S.; Koizumi, M. Ferrocyanide anion bearing Mg, Al hydroxide. *Mater. Res. Bull.* **1982**, *17*, 191-198, doi:https://doi.org/10.1016/0025-5408(82)90145-3.
93. Idemura, S.; Suzuki, E.; Ono, Y. Electronic State of Iron Complexes in the Interlayer of Hydrotalcite-Like Materials. *Clays Clay Miner.* **1989**, *37*, 553-557, doi:https://doi.org/10.1346/CCMN.1989.0370608.
94. Mao, G.; Tsuji, M.; Tamaura, Y. Synthesis and CO_2 Adsorption Features of a Hydrotalcite-Like Compound of the Mg^{2+}-Al^{3+}-$Fe(CN)_6^{4-}$ System with High Layer-Charge Density. *Clays Clay Miner.* **1993**, *41*, 731-737, doi:https://doi.org/10.1346/CCMN.1993.0410612.
95. Panda, H.S.; Srivastava, R.; Bahadur, D. Intercalation of Hexacyanoferrate(III) Ions in Layered Double Hydroxides: A Novel Precursor To Form Ferri-/Antiferromagnetic Exchange Coupled Oxides and Monodisperse Nanograin Spinel Ferrites. *J Phys Chem C* **2009**, *113*, 9560–9567, doi:https://doi.org/10.1021/jp8115066.
96. Meng, W., Li, F.; Evans, D.G.; Duan, X. Preparation and thermal decomposition of magnesium/iron(III) layered double hydroxide intercalated by hexacyanoferrate(III) ions. *J. Mater. Sci.* **2004**, *39*, 4655–4657, doi:https://doi.org/10.1023/B:JMSC.0000034164.42193.69.
97. Yao, K.; Taniguchi, M.; Nakata, M.; Shimazu, K.; Takahashi, M.; Yamagishi, A. Mass transport on an anionic clay-modified electrode as studied by a quartz crystal microbalance. *J. Electroanal. Chem.* **1998**, *457*, 119-128, doi:https://doi.org/10.1016/S0022-0728(98)00309-X.
98. Crespo, I.; Barriga, C.; Rives, V.; Ulibarri, M.A. Intercalation of iron hexacyano complexes in Zn,Al-hydrotalcite. *Solid State Ion.* **1997**, *101-103*, 729-735, doi:https://doi.org/10.1016/S0167-2738(97)00290-7.
99. Fernández, J.M.; Ulibarri, M.A.; Labajos, F.M.; Rives, V. The effect of iron on the crystalline phases formed upon thermal decomposition of Mg-Al-Fe hydrotalcites. *J. Mater. Chem.* **1998**, *8*, 2507-2514, doi:https://doi.org/10.1039/A804867C.
100. Gordon, B.M.; Williams, L.L.; Sutin, N. The Kinetics of the Oxidation of Iron(II) Ions and of Coördination Complexes[1a]. *J. Amer. Chem. Soc.* **1961**, *83*, 2061-2064, doi:https://doi.org/10.1021/ja01470a009.
101. Pelizzetti, E.; Mentasti, E.; Baiocchi, C. Kinetics and mechanism of oxidation of quinols by hexachloroiridate(IV) in aqueous acidic perchlorate media. *J. Phys. Chem.* **1976**, *80*, 2979-2982, doi:https://doi.org/10.1021/j100908a014.
102. Jones, L.H. Nature of Bonding in Metal Cyanide Complexes as Related to Intensity and Frequency of Infrared Absorption Spectra. *Inorg. Chem.* **1963**, *2*, 777-780, doi:https://doi.org/10.1021/ic50008a027.
103. Braterman, P.S.; Tan, C.; Zhao, J. Orientational effects in the infrared spectrum of the double layer material, magnesium aluminum hydroxide ferrocyanide. *Mater. Res. Bull.* **1994**, *29*, 1217-1221, doi:https://doi.org/10.1016/0025-5408(94)90144-9.
104. Boclair, J.W.; Braterman, P.S.; Brister, B.D.; Wang, Z.; Yarberry, F. Physical and Chemical Interactions between Mg:Al Layered Double Hydroxide and Hexacyanoferrate. *J. Solid State Chem.* **2001**, *161*, 249-258, doi:https://doi.org/10.1006/jssc.2001.9306.
105. Kloprogge, J.T.; Weier, M.; Crespo, I.; Ulibarri, M.A.; Barriga, C.; Rives, V.; Martens, W.N.; Frost, R.L. Intercalation of iron hexacyano complexes in Zn,Al hydrotalcite. Part 2. A mid-infrared and Raman spectroscopic study. *J. Solid State Chem.* **2004**, *177*, 1382-1387, doi:https://doi.org/10.1016/j.jssc.2003.11.034.